**ISTANBUL TECHNICAL UNIVERSITY ★ INSTITUTE OF SCIENCE AND TECHNOLOGY**

# SINGLE PHASE INDUCTION MOTOR SPEED CONTROL USING PWM AC CHOPPER FOR FAN APPLICATIONS

**M.Sc. Thesis by**
**Mustafa Murat BİLGİÇ**

**Department: Electrical Engineering**
**Programme: Electrical Engineering**

**Supervisor: Asst. Prof. Dr. Deniz YILDIRIM**

**JUNE 2007**

**İSTANBUL TECHNICAL UNIVERSITY ★ INSTITUTE OF SCIENCE AND TECHNOLOGY**

# SINGLE PHASE INDUCTION MOTOR SPEED CONTROL USING PWM AC CHOPPER FOR FAN APPLICATIONS

**M.Sc. Thesis by**
**Mustafa Murat BİLGİÇ**

**504041054**

**Date of submission : May 11, 2007**

**Date of defence examination: May 31, 2007**

**Supervisor (Chairman): Asst. Prof. Dr. Deniz YILDIRIM**

**Members of the Examining Committee Asst. Prof. Dr. Levent OVACIK**

**Asst. Prof. Dr. Metin AYDIN (KÜ.)**

**JUNE 2007**

**İSTANBUL TECHNICAL UNIVERSITY ★ FEN BİLİMLERİ ENSTİTÜSÜ**

# FAN UYGULAMALARI İÇİN TEK FAZLI ASENKRON MOTORUN DARBE GENİŞLİK MODÜLASYONLU AA KIYICISI HIZ KONTROLÜ

**Yüksek Lisans Tezi**
**Mustafa Murat BİLGİÇ**

**504041054**

**Tezin Enstitüye Verildiği Tarih: 11 Mayıs 2007**

**Tezin Savunulduğu Tarih: 31 Mayıs 2007**

**Tez Danışmanı : Yrd. Doç. Dr. Deniz YILDIRIM**

**Diğer Jüri Üyeleri : Yrd. Doç. Dr. Levent OVACIK**

**Yrd. Doç. Dr. Metin AYDIN (KÜ.)**

**HAZİRAN 2007**

**ACKOWLEDGMENTS**

In this thesis we have built a PWM AC Chopper induction motor drive. I would like to thank my supervisor Deniz YILDIRIM and my father Oruç BİLGİÇ for their supports in finishing my thesis. I would also like to thank my mother Vildan BİLGİÇ for her support with the cakes and wonderful foods she cooked. Thanks to my friends Evren Ozan GÖKSEL and Esin ALKAN for the toleration they have showed for my behavior during this study. Finally thanks to Ömer BAHÇIVAN, Recep ŞENYURT, Sait ÖZTÜRK and Sultan ÇAKAR from BAHÇIVAN ELECTRIC MOTORS COMPANY for their kind support in supplying equipment and cheer for this study.

JUNE 2007 Mustafa Murat BİLGİÇ

**TABLE OF CONTENTS**

**ABBREVIATIONS**

| | |
|---|---|
| **AC** | : Alternating Current |
| **DC** | : Direct Current |
| **PWM** | : Pulse Width Modulation |
| **SPIM** | : Single Phase Induction Motor |
| **SVPWM** | : Space Vector Pulse Width Modulation |
| **RMS** | : Root Mean Square |
| **EMI** | : Electromagnetic Interference |
| **EMC** | : Electromagnetic Compatibility |
| **FFT** | : Fast Fourier Transform |
| **NTC** | : Negative Temperature Constant |
| **PTC** | : Positive Temperature Constant |
| **MLT** | : Mean Length per Turns |

## LIST OF TABLES

**LIST OF FIGURES**

Page Numbers

## LIST OF SYMBOLS

| | |
|---|---|
| $T_e$ | : torque developed |
| $P$ | : pole number |
| $R_s$, $R_r$ | : stator and rotor resistances |
| $L_{ls}$, $L_{lr}$ | : stator and rotor leakage inductances |
| $r_m$, $r_a$ | : main and auxiliary resistances |
| $r_q$, $r_d$ | : *q* and *d* axis resistances |
| $r_c$ | : capacitor resistance |
| $L_m$, $L_a$ | : main and auxiliary inductances |
| $L_q$', $L_q$' | : *q* and *d* axis rotor resistance |
| $M_m$, $M_a$ | : main and auxiliary winding magnetizing inductances |
| $n$ | : turn ratio |
| $V_s$ | : effective value of the supply voltage |
| $\omega_e$ | : electrical speed in radians |
| $\Phi_m$ | : air-gap flux |
| $T_F$ | : firing time |
| $T_M$ | : modulation time |
| $T_{NF}$ | : OFF time |
| $I_L$, $V_L$ | : load current and load voltage |
| $V_g$ | : triggering signal |
| $V_m$ | : maximum supply voltage |
| α, β | : firing angle and extinction angle |
| $a_0$, $a_n$ and $b_n$ | : Fourier coefficients |
| $\omega_s$ | : switching frequency |
| $D$ | : duty cycle |
| $p$ | : *di/dt* |
| $\omega_r$ | : rotor mechanical speed in radians |
| $J$ | : inertia of the rotor |

# FAN UYGULAMALARI İÇİN TEK FAZLI ASENKRON MOTORUN DARBE GENİŞLİK MODÜLASYONLU AA KIYICISI HIZ KONTROLÜ

## ÖZET

Bu tezde fan uygulamalarında kullanılmak üzere tek fazlı sürekli kapasiteli bir asenkron motor için bir hız kontrol ünitesinin tasarımı ve gerçeklenmesi anlatılmıştır. Motorun girişine gelen alternatif geriliminin efektif değerini değiştirmek için darbe genişlik modülasyonlu (DGM) bir alternatif akım (AA) kıyıcısı kullanılmıştır. Böylece kaynak geriliminin efektif değeri ayarlanarak motorun hız kontrolü yapılmıştır. Fan uygulamasında devrenin kapalı çevrim çalışması için ısı geri beslemeli referans devresi oluşturulmuştur. Hız kontrol ünitesinde oluşan harmonik etkiler, TS EN 61000-3-2 harmonikli akım emisyon standartlarına bağlı kalınarak, bir giriş filtresi ile süzülmüştür. Devrede var olan entegrelerin bağımsız olarak beslenmesi için ayrıca düşük güçlü doğru akım (DA) kaynakları tasarlanmıştır.

## SINGLE PHASE INDUCTION MOTOR SPEED CONTROL USING PWM AC CHOPPER FOR FAN APPLICATIONS


## SUMMARY

This work presents a speed control unit for fan applications. A pulse width modulated (PWM) AC chopper that changes the effective value of the supply voltage applied to a single-phase induction motor. This variable supply voltage gives the ability to control the speed of the motor. For closed-loop operations a temperature feed-back reference circuit has been developed. Harmonics generated by the speed control unit are filtered by an input filter according to TS EN 61000-3-2 limits for harmonic current emissions standards. Design of low power supplies have been made in order to supply the IC's (integrated circuits) in the circuit.

# 1. INTRODUCTION

Induction motors are widely used in either industrial and domestic applications, especially for blower or fan applications due to their low costs, simple designs, easy to use and no need of maintenance.

The past years have brought standards for use and conservation of power, leading engineers all around the world to build low-power consumption. Therefore, this brings us to the importance of the control of induction motors.

Power electronic systems can produce low-cost, low-power consuming circuits to improve the use quality of the power used. This work introduces a speed control unit for fan applications.

## 1.1 Aim of Project

The aim of this project is, to control the speed of an induction motor in order to keep the temperature of a process at desired level by adjusting the rate of air flow.

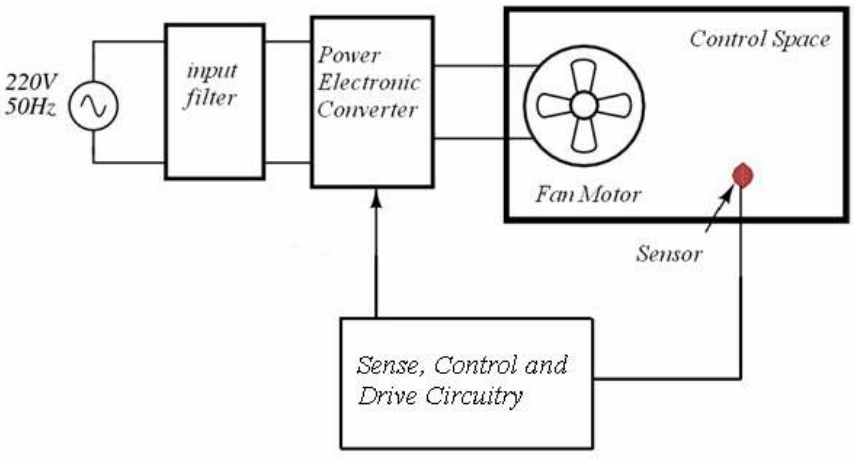


**Figure 1.1:** Temperature Control of a Process

The following chapters will present the path followed in order to reach this aim. The motor used in this project is a permanent split capacitor external-rotor single-phase induction motor.

### 1.2 Structure of Thesis

In the second section of this thesis, speed control techniques are investigated for single phase induction motors. Among these techniques, the pulse width modulated (PWM) AC chopper was selected for design.

The third section shows the path followed in the design of PWM AC chopper. This chapter presents a Pspice model of the AC chopper and a single phase induction motor model to analyze the performance of the chopper circuit under dynamic loads. Finally the realization of the AC chopper is discussed. Two different drive and isolation circuitry for the AC chopper are introduced in this section.

The fourth section presents the harmonic analysis of the circuit. Regarding to these analysis results a proper input filter for the chopper has been designed with respect to the international standards. The measurement and output graphs of the overall PWM AC chopper with input filter is shown in this section.

In the fifth section, temperature feed-back units for the closed loop operations are introduced. The design of a resistance-to-voltage converter is made by using a single operational amplifier.

In the appendixes the lists of materials used during the realization of the circuit are given. The design of an input filter inductor, auxiliary power supplies to feed the drivers and PWM generator and the pictures of the realized circuit are also given in the appendixes.

## 2. TECHNIQUES USED IN SINGLE PHASE INDUCTION MOTOR SPEED CONTROL

In this section, the techniques used in controlling single phase induction motors, the advantages and disadvantages of each control method are discussed. Depending on these results the reason why the PWM AC Chopper was selected for the speed control unit will be explained.

Two main techniques are used in single phase induction motor control. These are constant Volts-Per-Hertz (*V/f*) Control, Vector Control and Voltage Control techniques. The first, constant *V/f* control is designed to produce variable speed commands by using an inverter to apply a voltage of correct magnitude and frequency to approximately achieve the commanded speed. The vector control is referring not only to the magnitude but also to the phase of these variables. Matrix and vectors are used to represent the control quantities [1]. Finally, voltage control controls the speed of the motor by changing the effective value of the load voltage. There are three methods generally used in voltage control. These are phase control, integral cycle and PWM control.

### 2.1 Constant Volts – Per – Hertz (*V/f*) Control

As it is in the three phase induction motor, the single phase induction machine also has variable speeds for different frequency values. The constant *V/f* technique can also be used for controlling the single phase induction motor.

**T**he constant *V/f* control is widely used in the control in three phase induction motors. The torque developed ($T_e$) in a three phase motor; ignoring the magnetizing inductance and the iron loss, for constant supply voltage and frequency can be expressed in Equation 2.1,

$$T_e = 3\left(\frac{P}{2}\right)\frac{R_r}{s\omega_e}\frac{V_s^2}{\left(R_s + R_r/s\right)^2 + \omega_e^2\left(L_{ls} + L_{lr}\right)^2} \qquad \textbf{(2.1)}$$

where $P$ is the pole number, $s$ is the slip, $R_s$ and $R_r$ are the stator and rotor resistances respectively, $L_{ls}$ and $L_{lr}$ are the stator and rotor leakage inductances respectively, $V_s$ is the effective value of the supply voltage and $\omega_e$ is the electrical speed in radians.

And in steady state operations the air-gap flux $\Phi_m$ is related to the ratio $V/f$. Therefore, maintaining a constant air-gap flux will provide maximum torque sensitivity and stator current. It can be seen from Equation 2.1 that keeping the $V\backslash f$ ratio constant the air-gap flux can be kept constant, the Torque – Speed is shown in Figure 2.1.

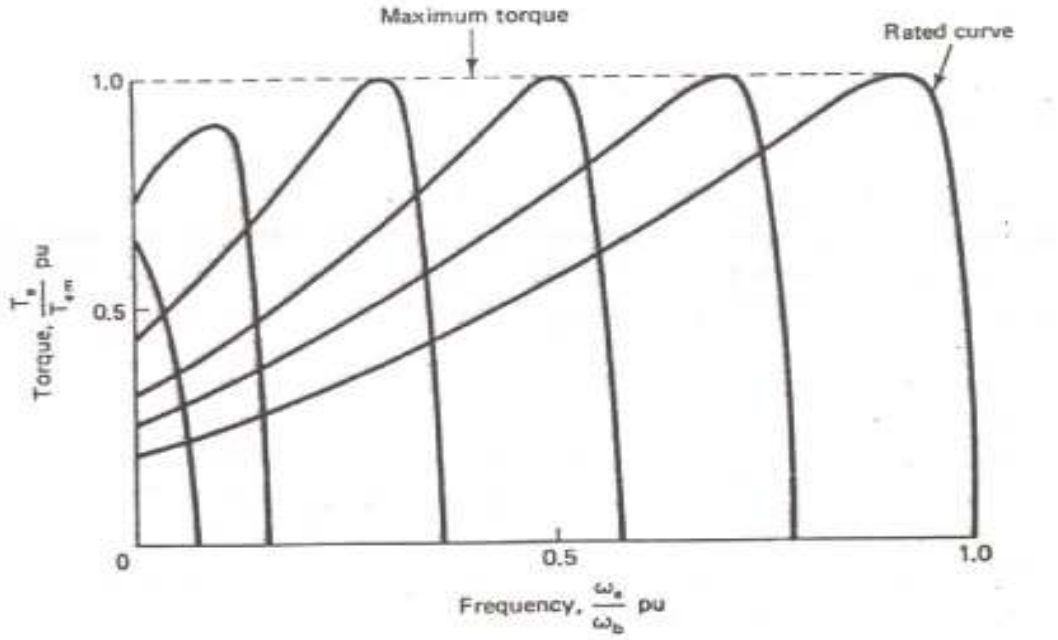


**Figure 2.1:** Torque-Speed Characteristic for Constant $V/f$ Control [2]

The torque equation $T_e$ given in Equation 2.1 remains approximately valid except in low-frequency region where air-gap flux is reduced due to the stator impedance drop. In low frequency region it is necessary to inject an auxiliary voltage $V_{aux}$ to overcome the effects of stator impedance so that the rated air gap flux and full torque can become available.

The general circuit diagram for open-loop constant volts-per-hertz control is shown in Figure2.2. The power circuit consists of a phase controlled rectifier with single- or three-phase ac power supply LC filter (DC link) and an inverter. [**2**]

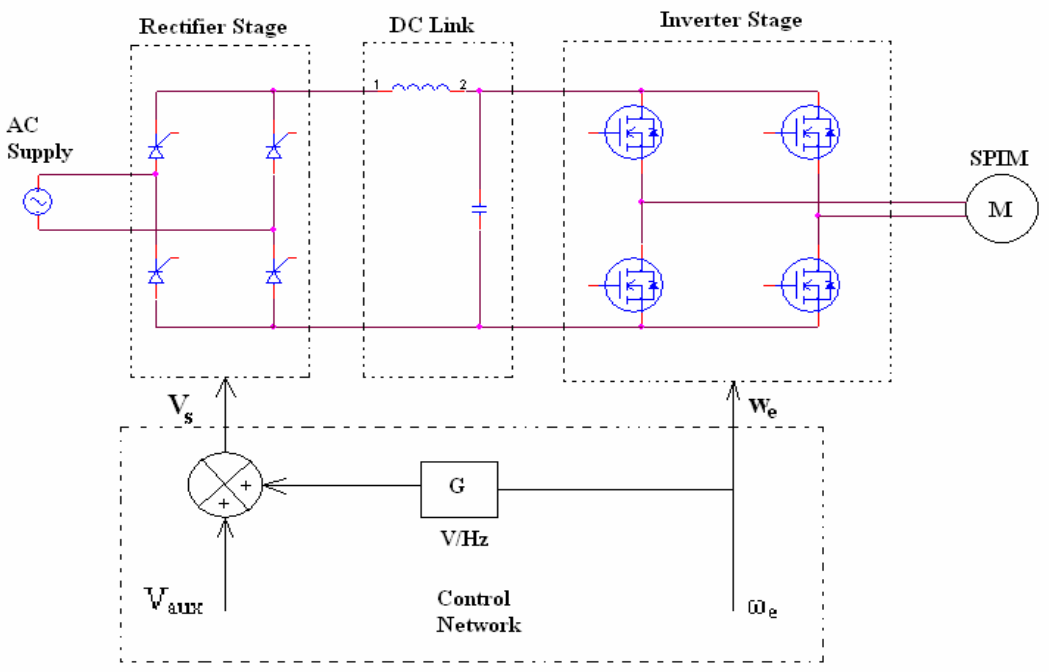


**Figure 2.2:** *V/f* Control Circuit Diagram [2]

## 2.2 Vector Control

The vector consists in controlling the components of the motor stator currents, represented by a vector, in a rotating reference frame *d, q* aligned with the rotor flux. The vector control system requires the dynamic model equations of the induction motor and returns to the instantaneous currents and voltages in order to calculate and control the variables [1].

The vector control of three-phase ac motors has mostly been used in servo systems due to its superior performance in spite of complexity. However, the vector control techniques for the single-phase induction motor drives have not been widely reported in literature in spite of several advantages. In reference [3] a single-phase Space Vector Pulse Width Modulation (SVPWM) technique is given. Figure 2.3 shows a single-phase half-bridge inverter for the single-phase induction motors and four space vectors used to control the switching pattern of the two-phase inverter.

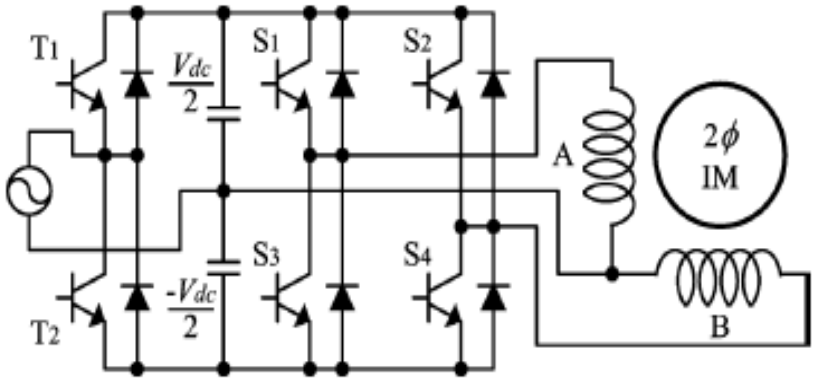


**(a)**

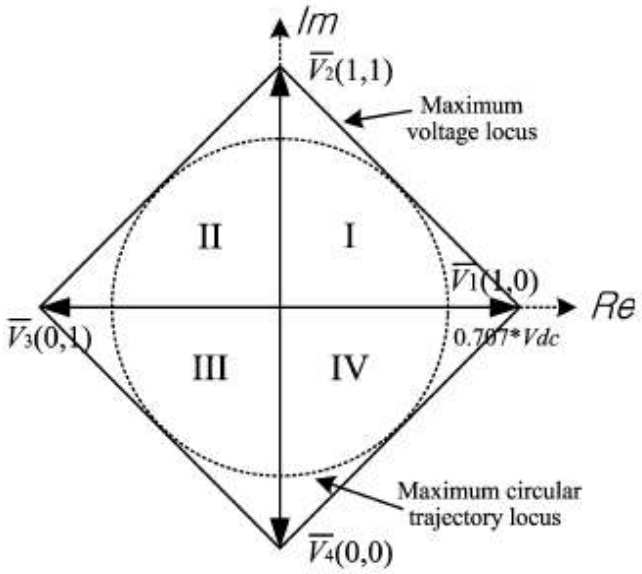


**(b)**

**Figure 2.3:** Vector Control of Single-Phase Induction Motors [3]; **(a)** Single-Phase Half Bridge Inverter, **(b)** Space Vectors of Single-Phase Induction Motor

## 2.3 Voltage Control

The speed of an induction motor can be controlled by changing the effective value of the stator voltage at constant frequency. Figure 2.4 is the Torque – Speed characteristic according to the Equation 2.1 for variable voltage.

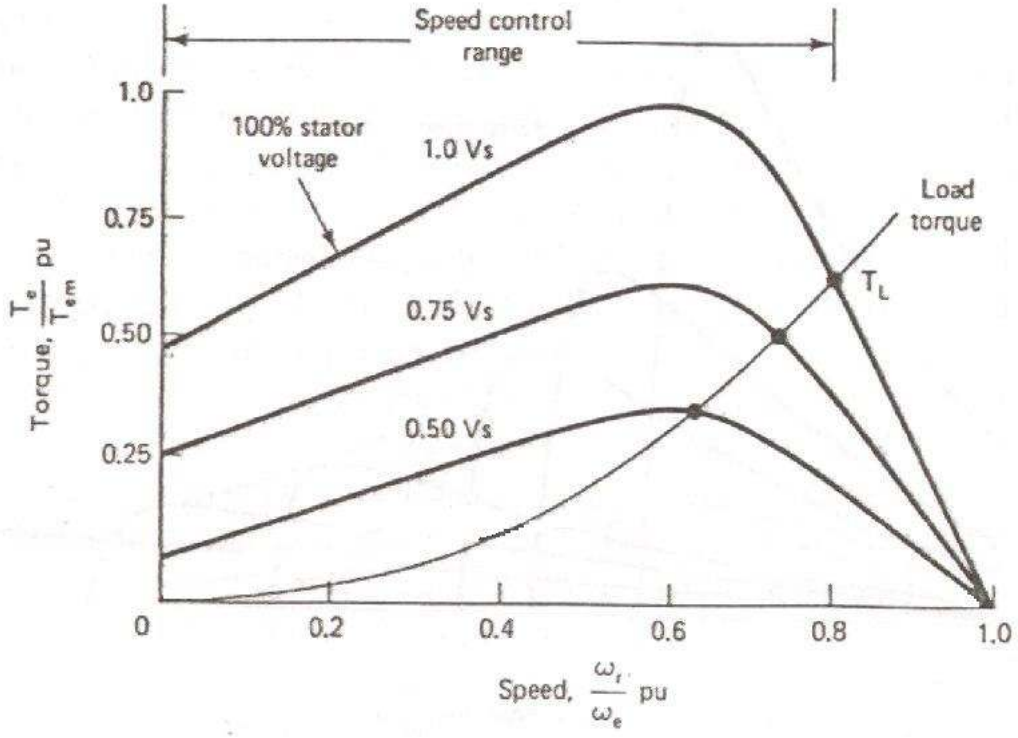


**Figure 2.4:** Voltage Control Torque – Speed Characteristic [2]

This method is mostly used in fan or blower type motors with high slip *s*. The speed control in this method operates by decreasing the air-gap flux value, therefore increasing the slip *s*.

The stator voltage can be controlled by three methods; integral cycle control, phase control and PWM control.

### 2.3.1 Integral Cycle Control

Integral Cycle Control is based on allowing certain number of complete cycles of the supply voltage to pass to the load. This can simply be done by turning on and off the source voltage. That is the reason why this technique is also called On-Off Control. Burst Fire Control, Single Cycle Control and Advanced Single Cycle Control are three different ways used in this technique.

### 2.3.1.1 Burst Fire Control

The Burst Firing mode consists of firing complete cycles of supply to the load.

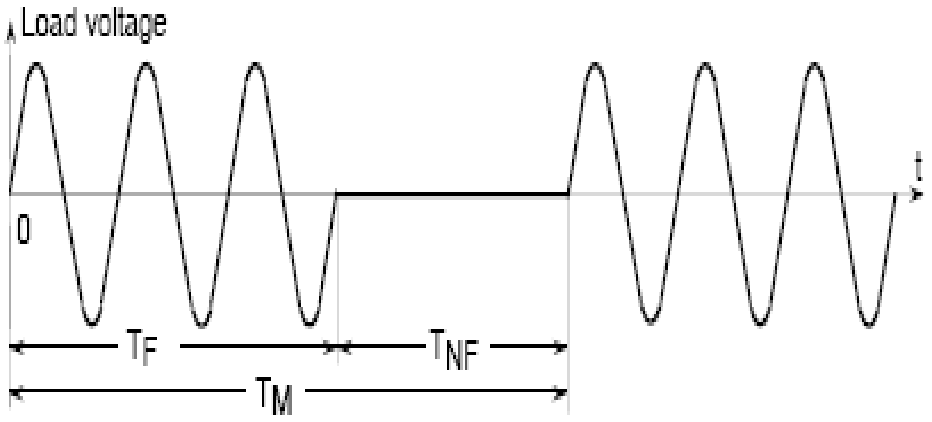


**Figure 2.5:** Burst Fire Control

The load power is proportional to the ratio of the firing time ($T_F$) to the modulation time ($T_M$). The OFF time ($T_{NF}$) is also a series of whole supply cycles.

$T_M = T_F + T_{NF}$

The RMS value of the load voltage is:

$$V_{L,rms} = V_{I,rms}\sqrt{\frac{T_F}{T_M}} \qquad \textbf{(2.2)}$$

where $V_{I,rms}$ is the effective value of the supply voltage.

For burst firing mode the firing time ($T_F$) is fixed to a certain time and the effective value of load voltage is changed by increasing or decreasing the off time ($T_{NF}$).

### 2.3.1.2 Single Cycle Control

The mode of firing with only one firing and one non-firing cycles is called the Single Cycle.

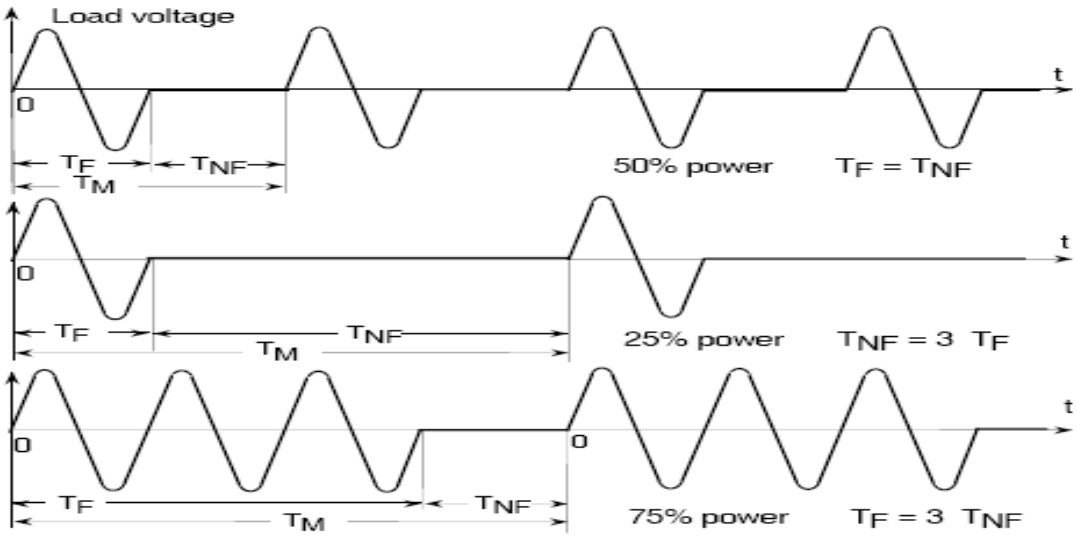


**Figure 2.6:** Load Voltage Waveform with Single Cycle Control

At 50% of nominal power the firing is adjusted so that the firing time ($T_F$) and non-firing times ($T_{NF}$) are equal. For a set point less than 50% power the Non-Firing time is increased and for a set point of power greater than 50% the firing time is increased.

### 2.3.1.3 Advanced Single Cycle Control

To reduce the power fluctuations during the modulation period, Advanced Single Cycle firing can be implemented using half cycle for non-firing.

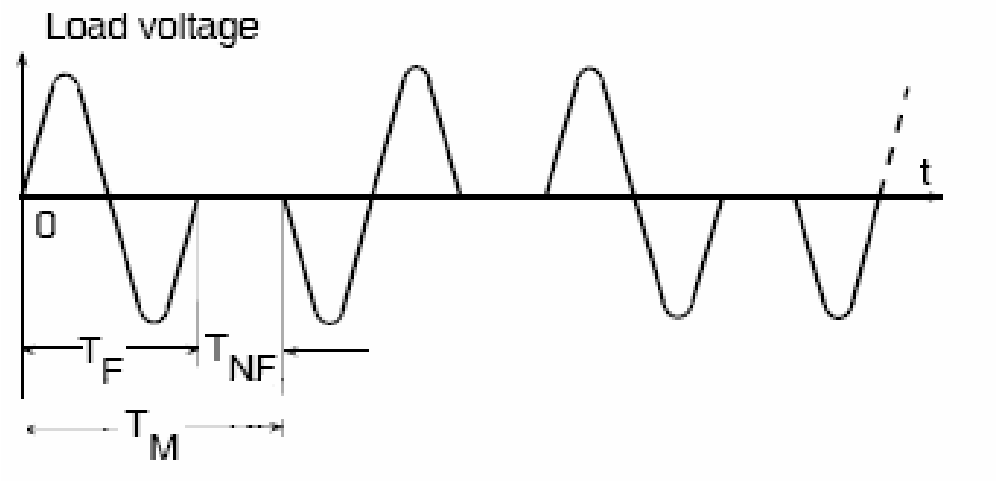


**Figure 2.7:** Load Voltage Waveform with Advanced Single Cycle Control

The effective value for Single Cycle and advance Single Cycle methods are both the same as which was given in Burst Firing mode.

### 2.3.2 Phase Control

Phase control is another voltage control technique where the power flow to the load is controlled by delaying the firing angles of the triac shown in Figure 2.8.

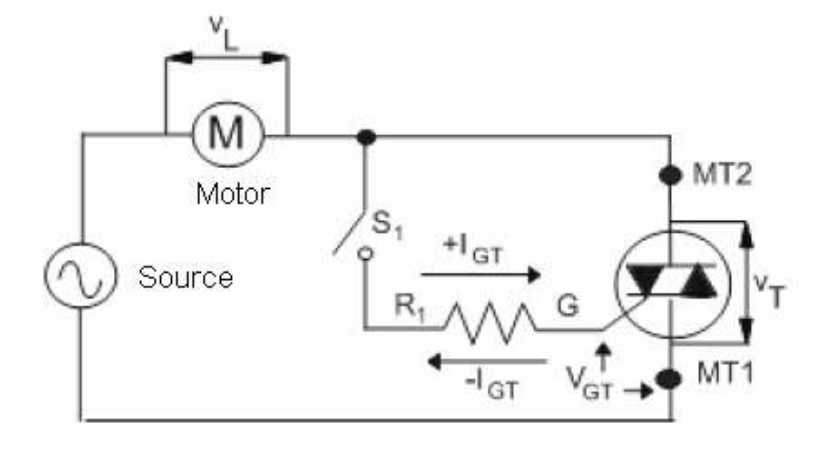


**Figure 2.8:** Phase Control Circuit [4]

When the triac is triggered the change in load current ($I_L$) and load voltage ($V_L$) are shown in Figure 2.9 according to the applied triggering signal ($V_g$).

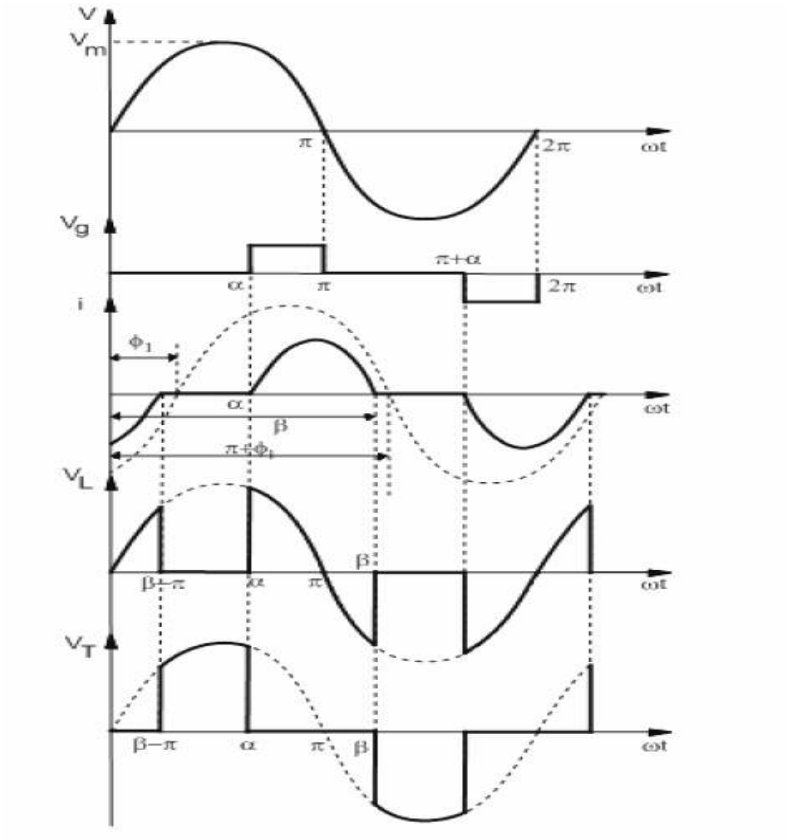


**Figure 2.9:** Phase Control Waveforms [4]

The RMS value of the load voltage ($V_L$) is as follows:

$$V_{L,rms} = V_m \sqrt{\frac{1}{2\pi}\left[(\beta - \alpha) + \frac{1}{2}\sin 2\alpha - \frac{1}{2}\sin 2\beta\right]} \quad \textbf{(2.3)}$$

where $V_m$ is the maximum supply voltage, α is the firing angle and β is the extinction angle.[4]

### 2.3.3 PWM Control

The PWM control technique simply chops the supply voltage at high frequencies as shown below in Figure 2.10.

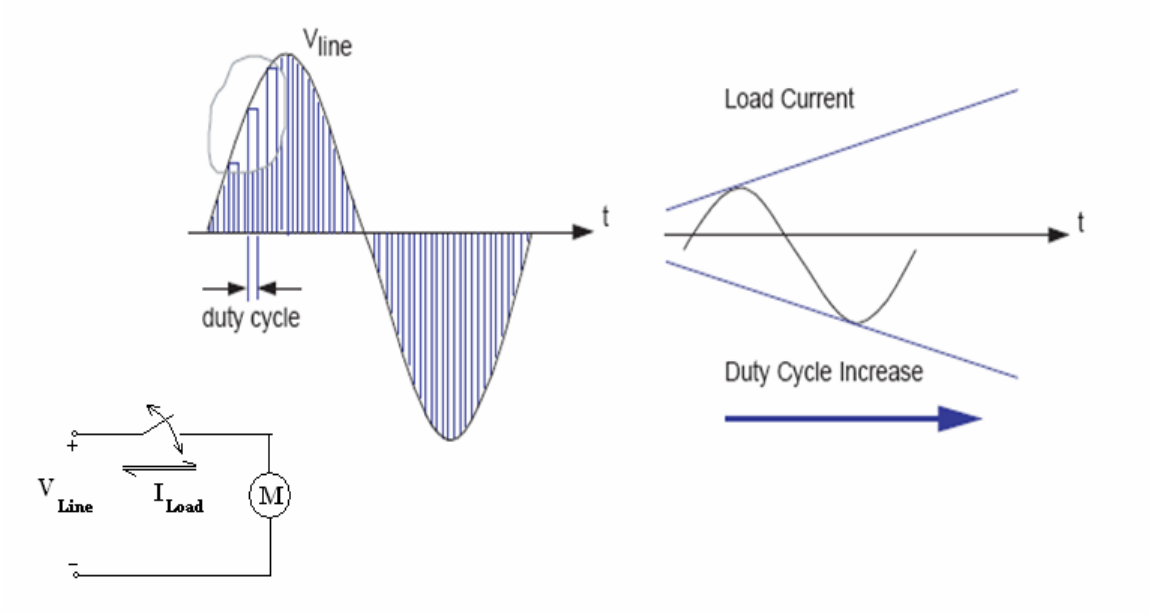


**Figure 2.10** PWM Chopping

The line voltage is chopped by a bi-directional switch. The change in the duty cycle of the switch changes the effective value of the load voltage and load current. The increase in duty cycle will allow the load current and load voltage to increase while decreasing the duty cycle will do the opposite effect to load current and load voltage.

The chopped voltage can be expressed by multiplying the sinusoidal line voltage with the switching signal shown in Figure 2.11 below.

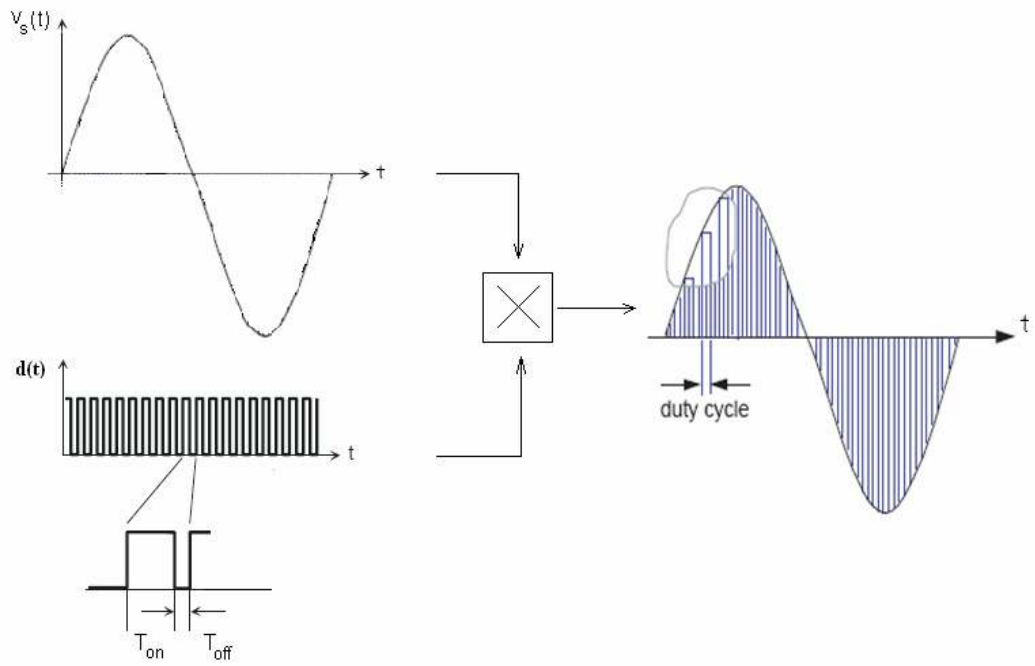


**Figure 2.11:** PWM Control Signals for Bi-directional Switching and Chopped AC Line Signal

The switching function can be written by opening the Fourier series of the pulse for one period.

$$d(t) = a_0 + \sum_{n=1}^{\infty}(a_n \cos n\omega_s t + b_n \sin n\omega_s t) \quad \textbf{(2.4)}$$

Where $a_0$ is the DC component, $a_n$ and $b_n$ are the Fourier coefficients and $\omega_s$ is the switching frequency. $a_0$, $a_n$ and $b_n$ have the following values.

$$a_0 = \frac{t_{on}}{T} = \frac{t_{on}}{t_{on} + t_{off}} = D \quad \text{duty cycle} \quad \textbf{(2.5)}$$

$$a_n = \frac{1}{\pi}\int_0^{2\pi} d(t)\cos(n\omega t)d\omega t \quad \textbf{(2.6)}$$

$$a_n = \frac{1}{n\pi}\sin(n2\pi D) \quad \textbf{(2.7)}$$

$$b_n = \frac{1}{\pi}\int_0^{2\pi} d(t)\sin(n\omega t)d\omega t \quad \textbf{(2.8)}$$

$$b_n = -\frac{1}{n\pi}\left[1 + \cos(n2\pi D)\right] \quad \textbf{(2.9)}$$

$$c_n = \sqrt{a_n^2 + b_n^2} \quad \textbf{(2.10)}$$

The load voltage can be calculated by multiplication of the supply voltage and switching function.

$$V_s(t) = V_m \sin \omega t \quad \textbf{(2.11)}$$

$$V_L(t) = V_s \cdot d(t) = V_m \sin \omega t \cdot d(t) \quad \textbf{(2.12)}$$

$$V_L(t) = a_0 V_m \sin \omega t + \left[\sum_{n=1}^{\infty} (a_n V_m (\cos n\omega_s t \cdot \sin \omega t) + b_n V_m (\sin n\omega_s t \cdot \sin \omega t))\right] \quad \textbf{(2.13)}$$

The terms in square brackets are the high frequency terms. When high frequency terms are filtered, the load voltage can be expressed according to the fundamental component supply frequency.

$$V_L(t) = a_0 V_m \sin \omega t = D.V_m \sin \omega t \quad \textbf{(2.14)}$$

The effective value of load voltage can be calculated easily as:

$$V_{L,rms} = \frac{D \cdot V_m}{\sqrt{2}} \quad \textbf{(2.15)}$$

### 2.4 Discussion

The control techniques introduced above are used in the control of single phase induction motors. Each control technique has advantages and disadvantages of its own which effects the selection of the control method. The machine used for speed control applications must also be considered, because different loads may cause different effects on the power converter dynamics.

The constant V/f control technique is known to be one of the best control methods for speed control applications. Since the motor is operated at a constant air-gap flux in the constant torque region, the machine has a low slip characteristic giving improved efficiency. Despite all of these advantages the use of this technique is not

effective for this application because it beholds too many components, increasing the cost and a complex control network.

The vector control is a high performance control method mostly used in three-phase induction motors. This technique can be used on single-phase induction motors, too. But the control circuit is much more complex then three-phase induction motor vector control or constant *V/f* control.

On the other hand, the voltage control technique is much simpler in structure easy to control and cost efficient. Because of these reasons it is preferred in the industry for fan and blower applications. This technique is based on varying the slip rate, which is the difference between rotors actual speed and synchronous speed. The increase in the slip rate causes the speed to decrease. The increasing stator currents lead to more copper loss and machine heating.

It is necessary in motor drive circuits to apply a continuous current to the motor in order to protect the motor from electro-magnetic moment pulsations and speed oscillations. Motors having high inertia may be harmed from these oscillations.

The integral cycle (On-Off) control is based on supplying and cutting the supply currents, leading to discontinuities in the motor current which is a disadvantage in using this control method. This problem can be improved by increasing the total on and off time. One other effect of discontinuing currents in integral cycle control is that each control cycle the stator voltage is reduced to zero and again increased to the supply voltage value which increases the transient effects of the motor which is not desired.

In phase control the motor current is much more continuous compared to the integral cycle control, but still has discontinuity.

In PWM voltage control and constant V/f control the motor currents are nearly pure sinusoidal with very small harmonics. This result brings an advantage to these two control method compared with phase and integral cycle control.

Another important subject in the speed control methods mentioned before is the harmonics produced in the power converter stage.

The Integral cycle control method controls the voltage without deformation. This results to having no harmonics greater than the fundamental component at 50Hz

which appears to be a good advantage. Since the operation frequency is decrease to less than 50Hz due to the on and off firing times, the integral cycle control produces sub-harmonics having greater magnitude than the fundamental harmonic. These sub-harmonics can not be filtered easily and creates major problems due to overheating caused by excessive currents of low frequencies less than 50Hz.

On the other hand voltage control techniques the supply voltage is deformed in order to decrease the effective value. In Phase control a switching frequency at 50Hz causes odd multiple harmonics of the supply frequency which somehow can be reduced by a relatively large filter. As mentioned before the load current supplied by the converter is discontinuous causing current harmonics to the motor. These harmonic currents must also be filtered for the protection of the machine.

PWM control using AC chopper is a good solution in terms of harmonics. Since high frequency switching (greater than 20 kHz) is used, current harmonics at the output of the converter are filtered by the motors inner inductance that results a nearly pure sinusoidal current. Compared to phase control the first harmonic appears much higher than the fundamental component. This reduces the size of the inductor, and simplifies the LC filter.

As far as the harmonics are concerned the best solution would be *V/f* control. The switching pattern in constant *V/f* control is based on harmonic reduction. Due to symmetric properties and the arrangement in triggering angles in the switching signal, the harmonics are reduced at the output and provide a continuous current to the motor.

Besides all of its good advantages the constant *V/f* control was not selected for this application due its complex control network and high cost. On the other hand PWM controlled AC Chopper suits best for this application for its simple structure, ease of control and high performance compared to the other voltage control techniques.

## 3. THE PWM AC CHOPPER

In this part the basics and design of the PWM AC Chopper is introduced. Before realizing, the PWM AC Chopper was first designed on Pspice AD simulator and a single phase induction motor Pspice modeled was developed in order to use a proper load. The simulation results are then compared with the experimental PWM AC Chopper circuit. An alternative circuit is also introduced here with the same working principles but different drive and isolation circuitry.

The PWM AC Chopper is actually a Buck converter operating in AC mode (Figure 3.1). It is made of two bi-directional switches with complementary switching patterns. The upper switch (SW1) is for voltage chopping and the lower switch (SW2) is placed to make a discharge path for the energy stored in the inductance of the motor while SW1 is open.

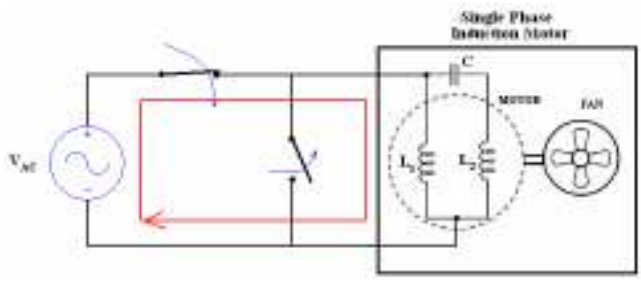

**(a)**

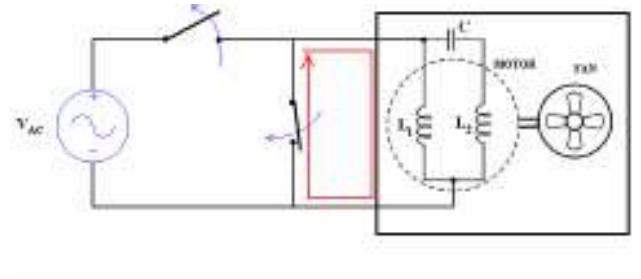

**(b)**

**Figure 3.1:** A Simple Single-Phase AC Chopper ($L_1$: main winding, $L_2$: auxiliary winding, $C$: permanent-split capacitor); **(a)** Current Flow Path when Upper Switch is ON, **(b)** Current Flow Path when Lower Switch is ON

The bidirectional switch is a switch capable of passing current in both directions thus allowing power to flow in both directions. An ideal bidirectional switch and a simplified model are shown in Figure 3.2 as follows.

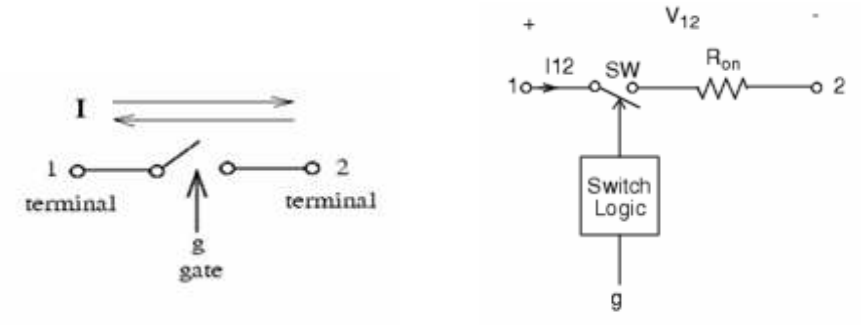


**(a)** **(b)**

**Figure 3.2:** Bi-directional Switch [5]**;**
**(a)** Ideal Bi-directional Switch, **(b)** Simplified Bi-Directional Switch

There are many ways of realizing bidirectional switches using power semiconductors. In Figure 3.3 some configurations are shown of realizing bidirectional switches by using power semiconductors. These power semiconductors can be power MosFETs, tyristors and insulated gate bipolar transistors (IGBT) and power bipolar transistors (BJT).

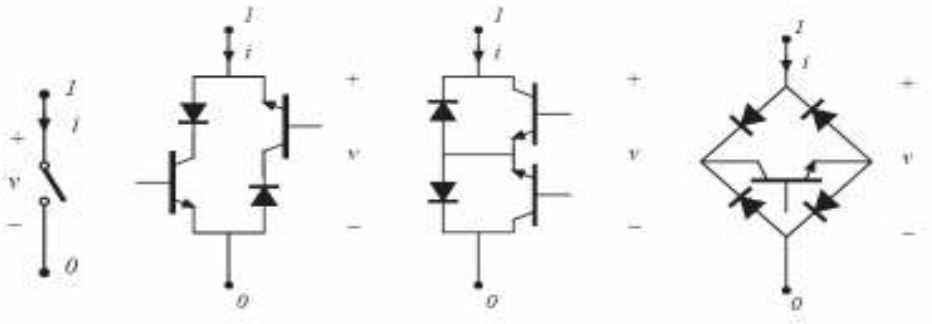

**Figure 3.3:** Realization of Bi-directional Switches
with Power Semiconductors [5]

In both simulations and experimentations, the bidirectional switches were realized with power MosFETs. Figure 3.4 shows the general topology of the PWM AC Chopper speed control circuit with temperature feedback.

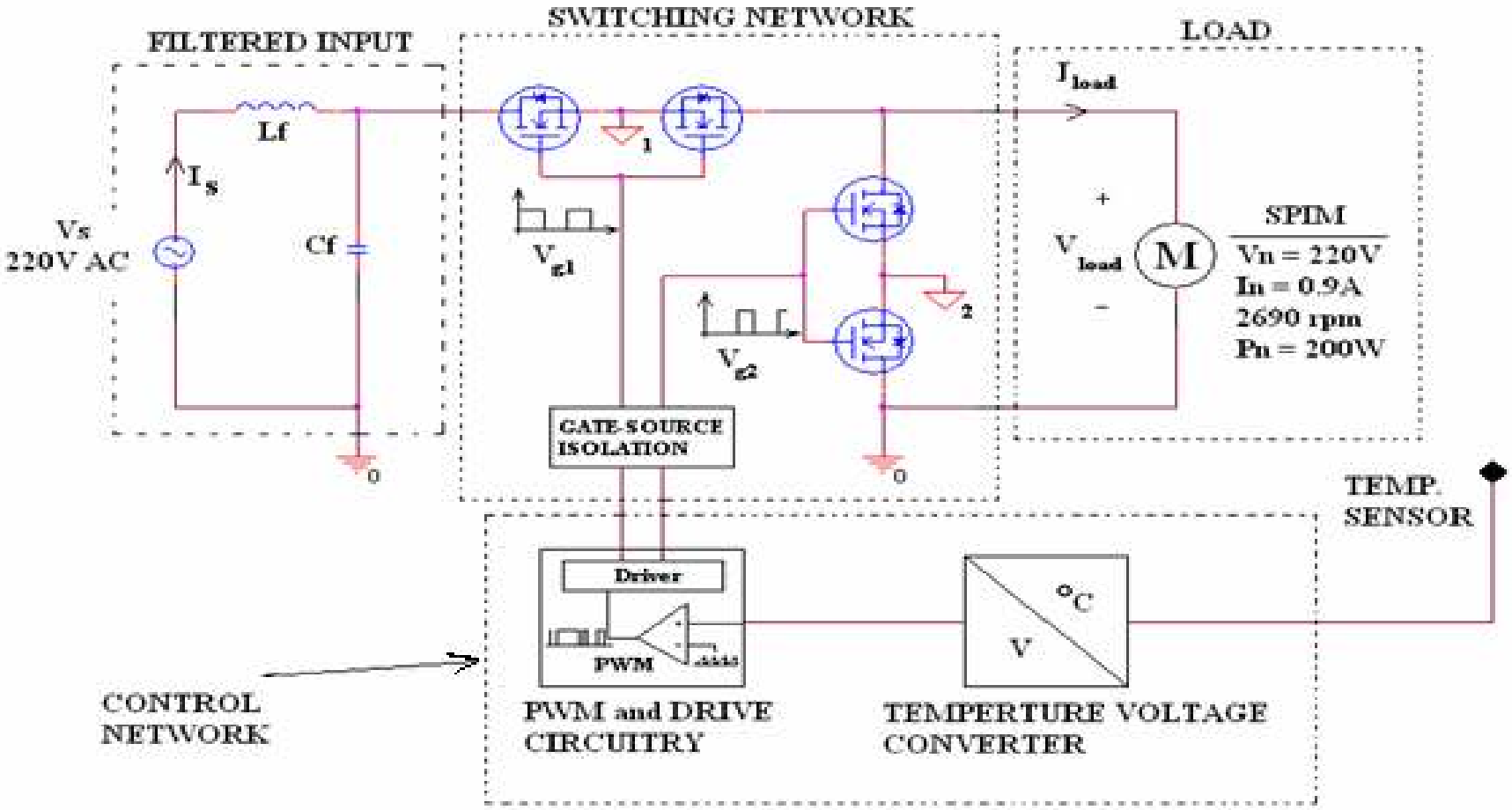


**Figure 3.4:** PWM AC Chopper Realized with Power MosFETs

Figure 3.4 shows the general configuration of the PWM AC Chopper. Temperature is sensed and converted to voltage which is the reference signal of the PWM generator. This reference signal is compared with a triangle wave which oscillates at high frequency. The comparator output is a pulse width modulated signal according to the reference signal. These modulated signals are passed to a simple driver capable of generating two complementary gate signals for the MosFETs in the switching network.

Both switches in the switching network are floating switches. To drive this switch, the converter stage and the control network must be isolated. This isolation can be done by implementing a pulse transformer or an optic coupler.

The input filter stage filters the high frequency switching harmonics from entering the utility. The filtered input is chopped in the switching network with the necessary duty cycle for the speed requirements and passed.

## 3.1 Modeling of Complete System

Orcad Pspice AD simulator was used to simulate the proposed circuit. Since the AC chopper will control a single-phase induction motor, a proper single-phase induction machine Pspice model was used. The following sections will show these Pspice Models in three parts; the single-phase induction motor model, the AC Chopper and the PWM generator.

### 3.1.1 Single Phase Induction Motor Pspice Model

When the voltage equations those describe a three-phase induction motors performance is investigated [6], it can be found that some of the machine inductances are functions of the rotor speed whereupon the coefficient of the voltage equations are time varying except when the rotor is stalled. A change of variables is often used to reduce the complexity of these differential equations. This change is a transformation of machine variables to frame of reference that rotates at an arbitrary angular velocity. This transformation applied to three-phase motors can also be applied to single-phase induction motors.[6] The following model used in simulation was taken from reference[7]. This model transforms the dynamic voltage equations of a single-phase induction motor into the arbitrary rotating *d-q* reference frame axis.

Figure 3.5 shows the arbitrary d-q axis and the motor components placed on this frame.

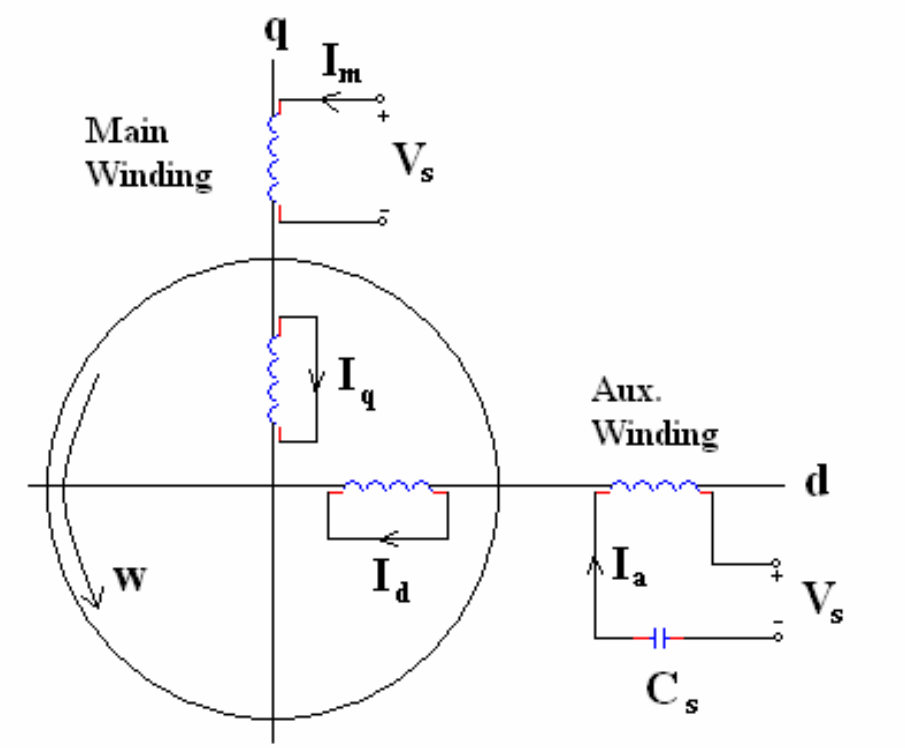


**Figure3.5:** Permanent Split-Capacitor Single-Phase Induction Motor [7]

The following equations are the transformed dynamic voltage equation to the d-q axis shown in Figure 3.5.

Main Winding: $$v_s = r_m i_m + L_m p i_m + M_m p i'_q \quad \textbf{(3.1)}$$

Aux. Winding: $$v_s = r_c i_a + p^{-1} i_a / C + r_a i_a + L_a p i_a + M_a p i'_d \quad \textbf{(3.2)}$$

Rotor q winding: $$0 = M_m p i_m - M_a \omega_r i_a / n + r'_q i'_q + L'_q p i'_q - L'_d \omega_r i'_d \quad \textbf{(3.3)}$$

Rotor d Winding: $$0 = M_a p i_a + n M_m \omega_r i_m + r'_d i'_d + L'_d p i'_d + n L'_q \omega_r i'_q \quad \textbf{(3.4)}$$

Torque Equation: $$T_e = PnM_m \left[ i_m i'_d - i_a i'_q \right] = T_j + \frac{J}{P}\left( \frac{d\omega_r}{dt} \right) \quad \textbf{(3.5)}$$

where $p = di/dt$, $T_e$ is the developed torque, $v_s$ is the effective value of the supply voltage, $r_m$ is the magnetizing resistance, $r_c$ is the capacitor resistance, $r_a$ is the

auxiliary winding resistance, $r_q$ is the rotor bars $q$ axis resistance, $r_d$ is the rotor bars $d$ axis resistance, $L_m$ is the main winding inductance, $L_a$ is the auxiliary winding leakage inductance, $L_d'$ is the rotor $d$ axis leakage inductance, $L_q'$ is the rotor $q$ axis leakage inductance, $M_m$ is the main winding magnetizing inductance, $M_a$ is the auxiliary winding magnetizing inductance $i_m$ is the main winding current, $i_a$ is the auxiliary winding current, $i_q'$ is the rotor $q$ axis current, $i_d'$ is the rotor $d$ axis current, $n$ is the turn ratio between main and auxiliary winding, $P$ is the pole number, $J$ is the inertia of the rotor and $\omega_r$ is the rotor mechanical speed.

All parameters due to rotor $q$ winding are referred to stator $m$ winding, all parameters due to rotor $d$ winding are referred to stator $a$ winding. Self inductances and mutual inductances of the motor are as follows:

$$\begin{aligned} L_m &= M_m + L_{lm} \\ L_a &= M_a + L_{la} \\ L_q' &= M_m + L_{lq}' \\ L_d' &= M_a + L_{ld}' \end{aligned} \qquad \textbf{(3.6)}$$

The system described by these equations can be represented in an equivalent circuit shown in Figure 3.6.

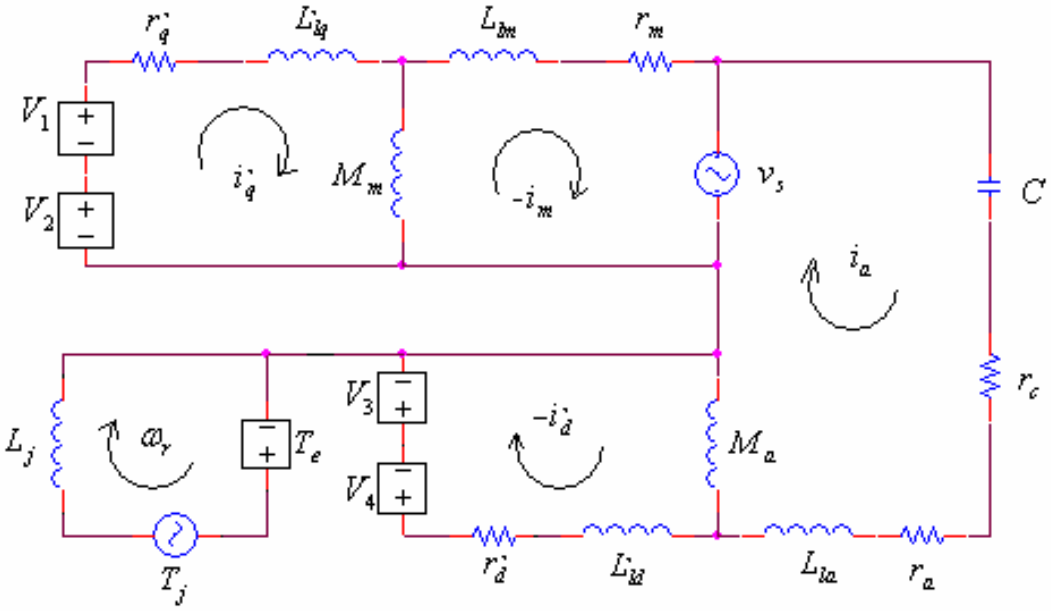


**Figure 3.6:** Dynamic Equivalent Circuit of Single Phase Induction Motor

Sources $V_1$, $V_2$, $V_3$ and $V_4$ are current dependent voltage sources. Voltage current relations of these sources are:

$$V_1 = M_a \omega_r \, i_a / n \tag{3.7}$$

$$V_2 = L_d' \omega_r \, i_d' / n \tag{3.8}$$

$$V_3 = n M_m \omega_r i_m \tag{3.9}$$

$$V_4 = n L_q' \omega_r i_q' \tag{3.10}$$

$$T_e = P n M_m \left[ i_m i_d' - i_a i_q' \right]. \tag{3.11}$$

The motor used in the model for simulation is not the motor used in experimentations. When comparing the simulation results with experimental results, there will be differences in magnitudes but the waveforms will be the same. The simulation results will only give a view on the behavior of the AC chopper for dynamic loads.

The motor used is a 110V, 60 Hz, 0.25 hp, 4-pole single-phase induction motor rest of the parameters can be seen on Table 3.1. The following figures show results of the single-phase induction machine model due to these parameters.

**Table 3.1:** Parameters of Motor used in Simulation [7]

| Name | Value |
|---|---|
| **Main Winding Components** | |
| $r_m$ | 2,02 Ω |
| $X_{lm}$ | 2,79 Ω |
| **Auxiliary Winding Components** | |
| $r_a$ | 7,14 Ω |
| $X_{la}$ | 3,22 Ω |
| **Field Winding Components** | |
| $r_q'$ | 4,12 Ω |
| $r_d'$ | 5,74 Ω |
| $X_{lq}'$ | 21,2 Ω |
| $X_{ld}'$ | 2,95 Ω |
| **Magnetization Reactance** | |
| $X_{mm}$ | 66,8 Ω |
| $X_{ma}$ | 92.9 Ω |
| **Winding Turn Ratio** | $n$ = 1,18 |
| **Moment of Inertia** | $J$ = 0,0146 kg.m$^2$ |
| **Capacitor** | 35 µF |

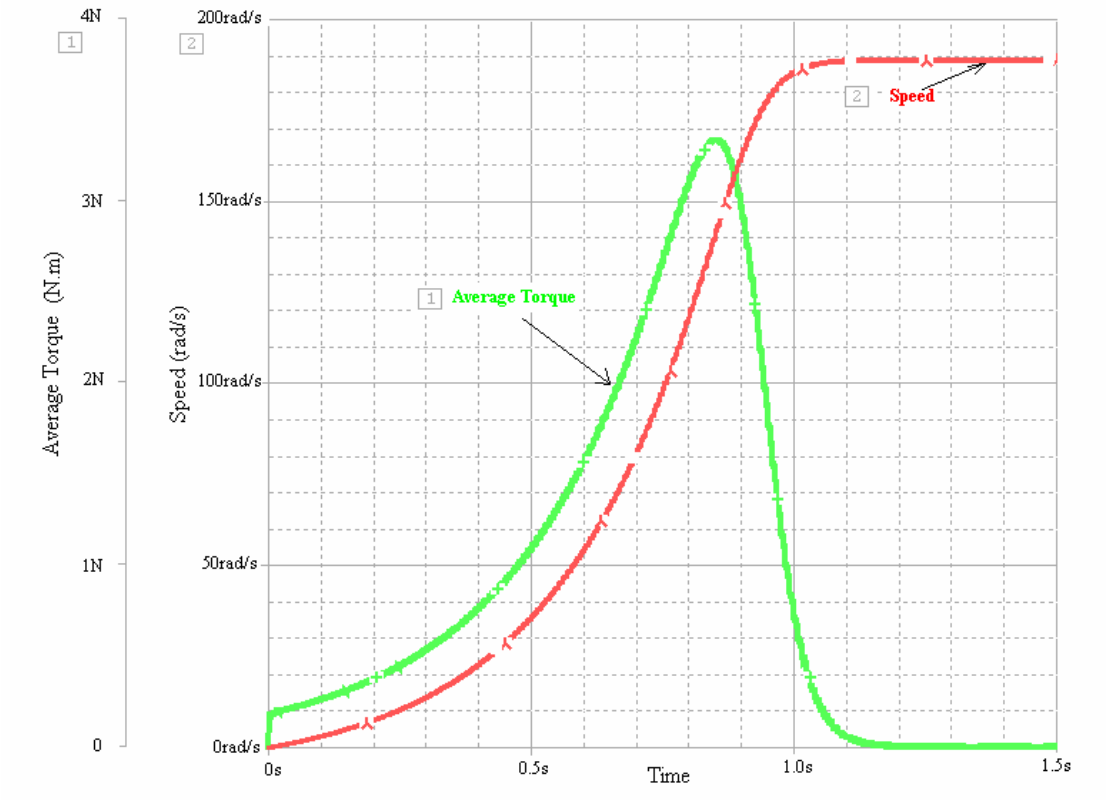


**Figure 3.7:** Simulation Results of Average Torque and Speed

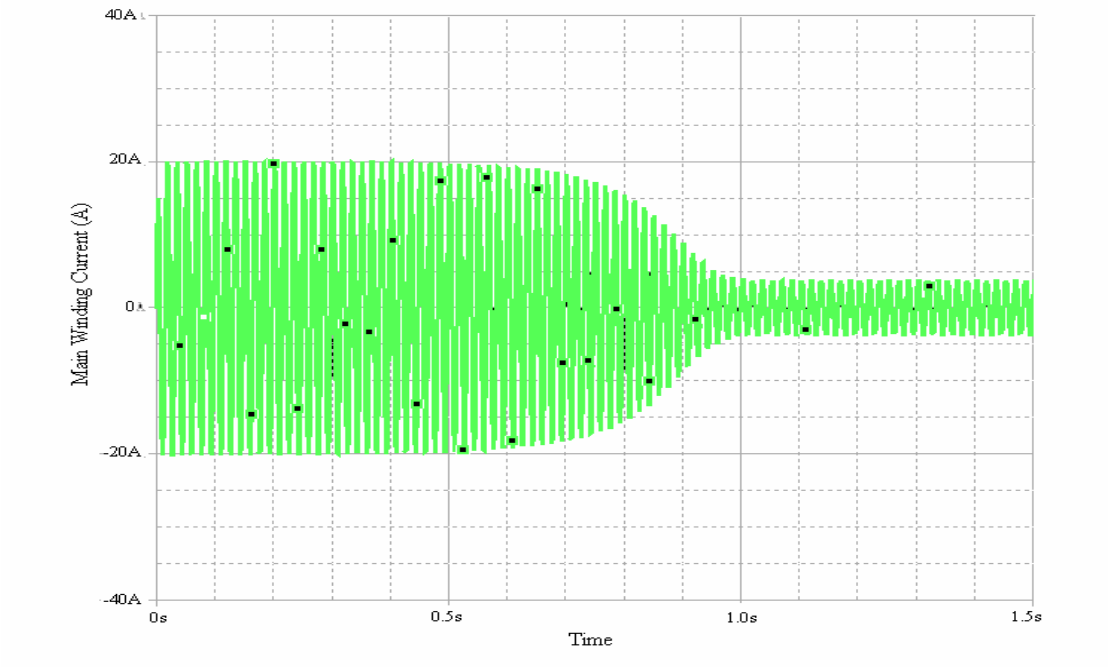


**Figure 3.8:** Simulation Results of Main Winding Current

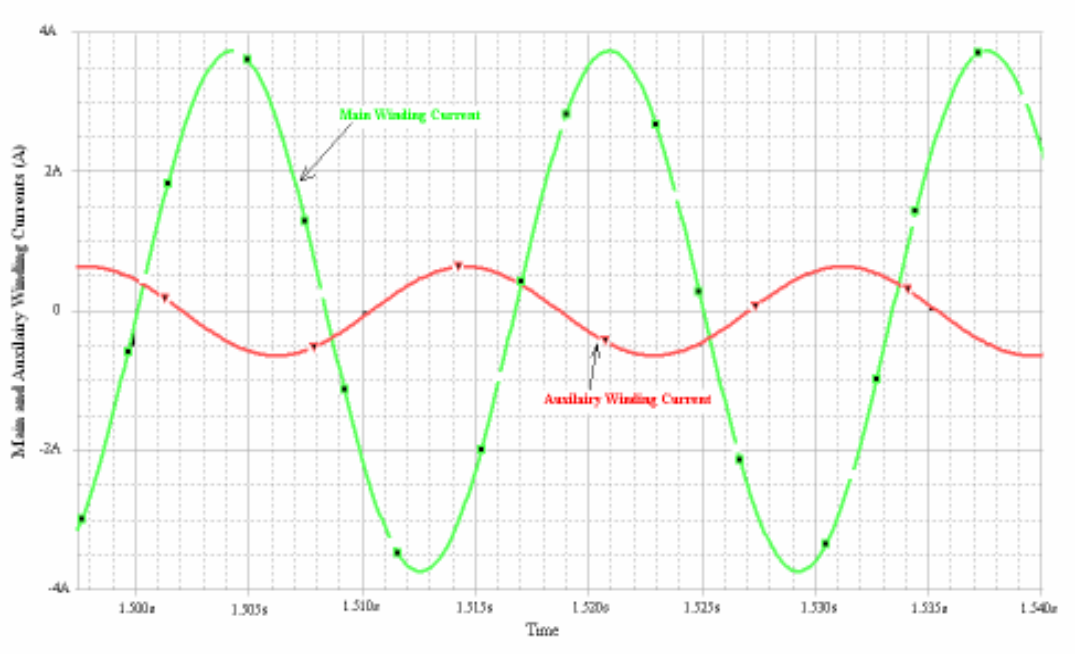


**Figure 3.9:** Simulation Results of Main and Auxiliary Winding Currents (Detailed view at Steady State)

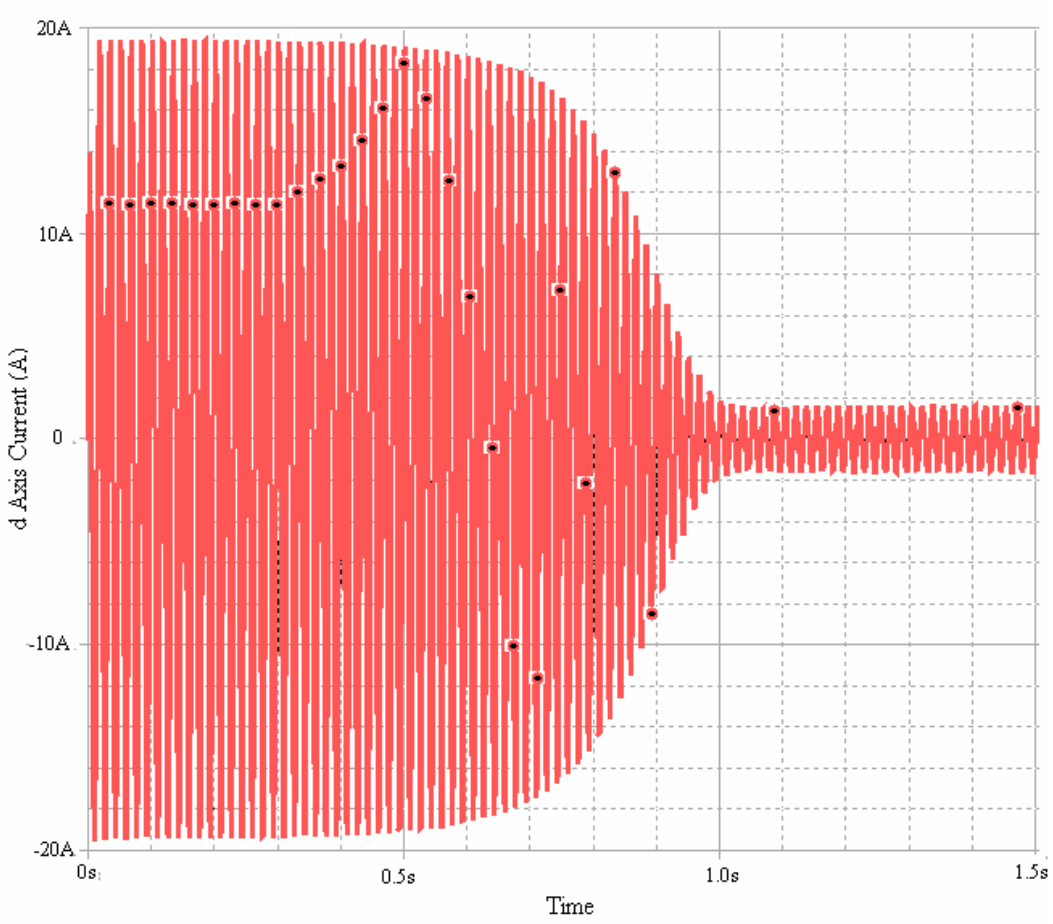


**Figure 3.10:** *d* Axis Current

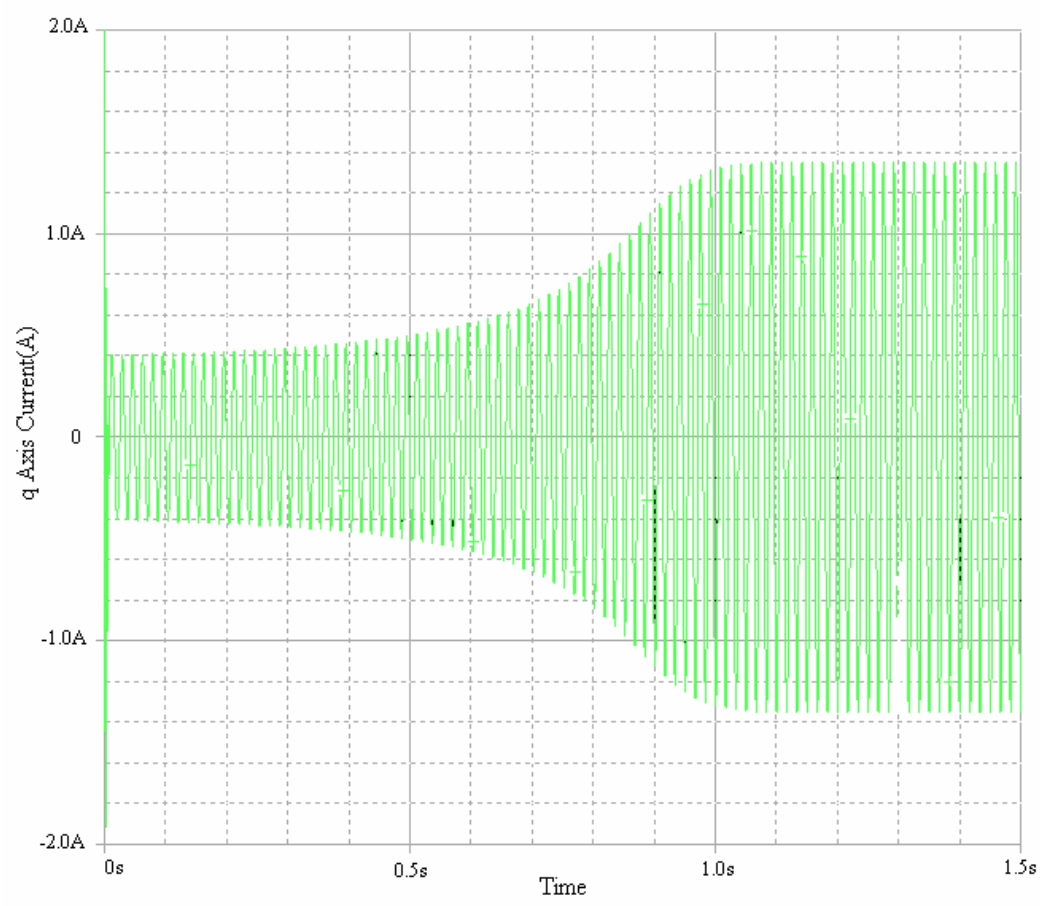


**Figure 3.11:** *q* Axis Current

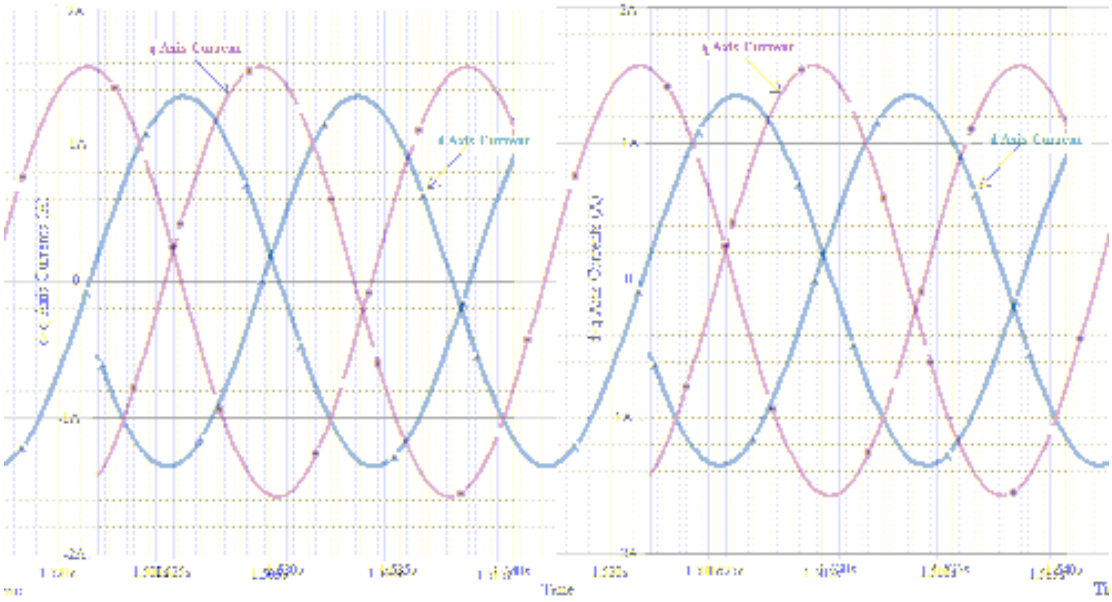

**Figure 3.12:** *d-q* Axis Currents (detailed view at stead state)

### 3.1.2 PWM AC Chopper

The PWM AC chopper spice model was designed referring to Figure 3.4. The Motor model was placed in the circuit as a sub circuit. Figure 3.13 and Figure 3.14 shows the spice schematics of the AC chopper and PWM Generator.

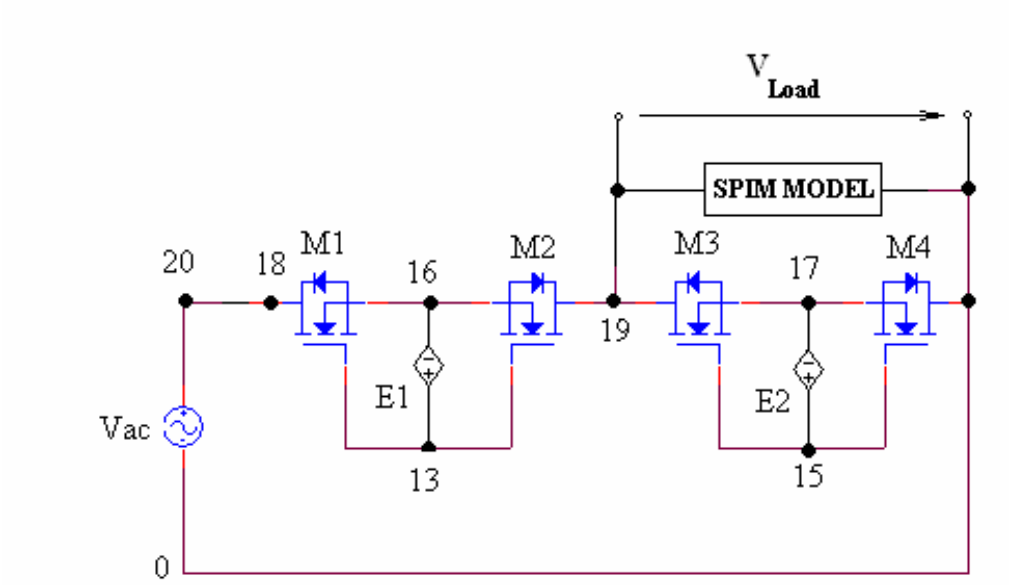


**Figure 3.13:** AC Chopper Pspice Schematics

Bi-directional switches are realized by $M_1$, $M_2$, $M_3$ and $M_4$ MosFETs. The gate-source of bi-directional switches is isolated using dependent voltage sources. $E_{1,ref}$ and $E_{2,ref}$ are reference signals are generated at the output of the PWM generator shown in Figure 3.14.

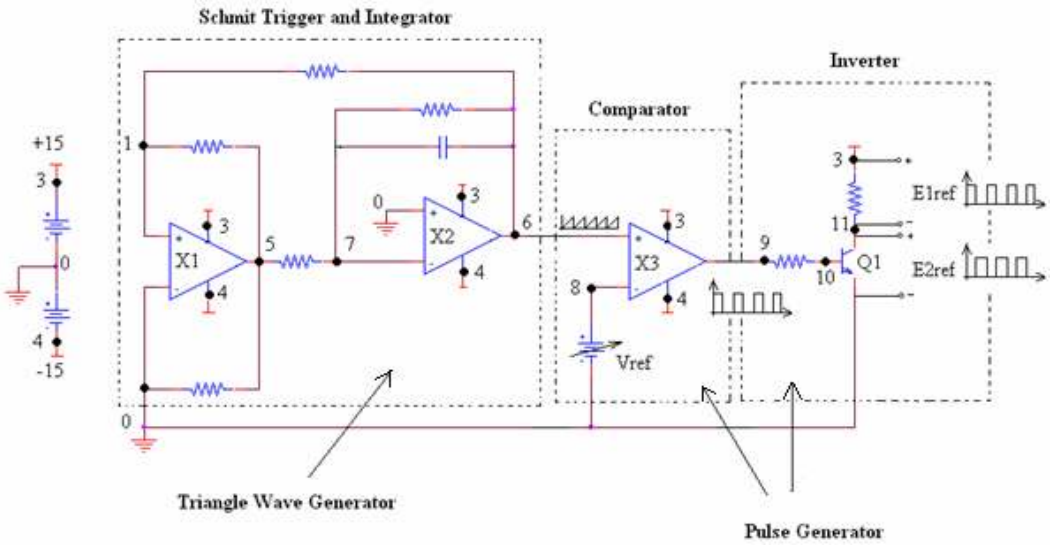


**Figure 3.14:** PWM Generator

The PWM generator was constructed using operational amplifiers for better modeling. The PWM generator is built up of a Schmit Trigger – Integrator Pair to generate the triangular wave which is compared with a reference voltage $V_{ref}$ by a comparator. The output modulated pulse is sent to the input of a BJT inverter. The outputs of this inverter give us 2 complementary signals which are used to drive the MosFETs. For $V_{ref}$ 0 which makes duty cycle 0.5 the simulation results are shown bellow.

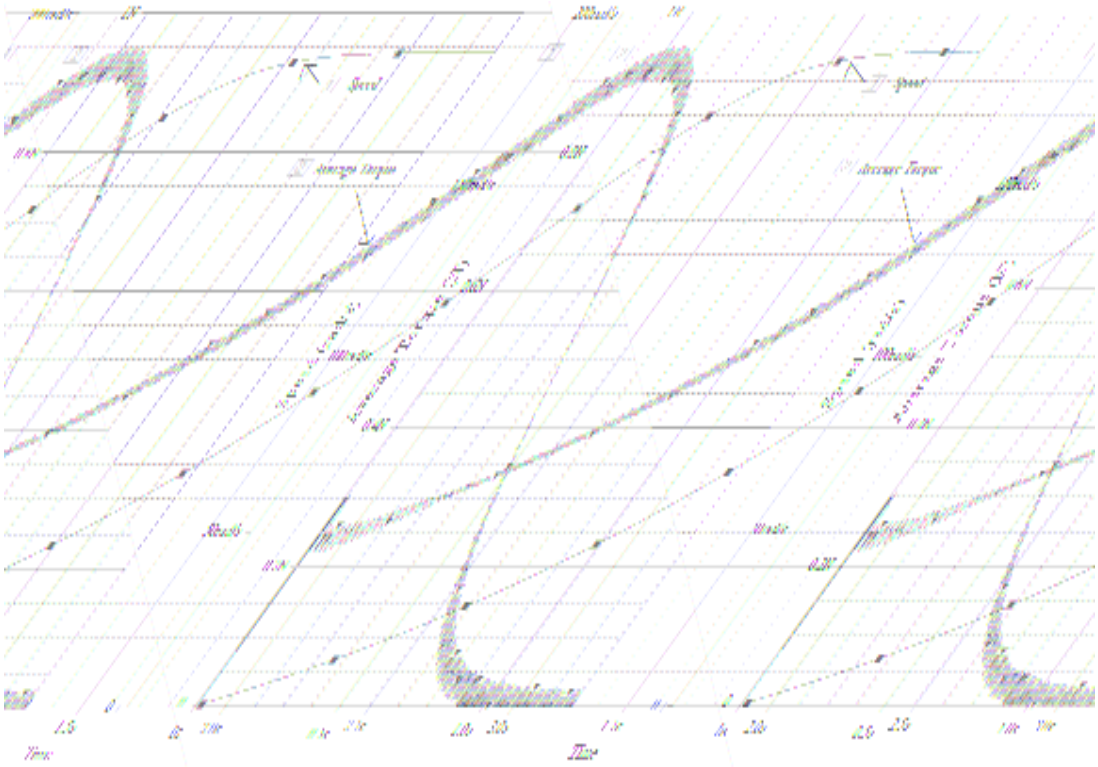

**Figure 3.15:** Torque and Speed Graph at D = 0.5

Figure 3.15 shows the torque and speed and graphs at duty cycle 0.5 under no load conditions. When no load is applied the speed of the rotor will try to reach synchronous speed. The motor applied to the Ac Chopper as load is a single-phase 110V, 60Hz 4 pole induction motor. Therefore the synchronous speed will be 180rad/s. When the average torque of Figure 3.15 is compared to the average torque value on Figure 3.7 it is seen that the torque value has decreased due to chopping of the line voltage. Figure 3.16 shows the output voltage of chopper and the pure sinusoidal load current drawn by the motor.


(a)

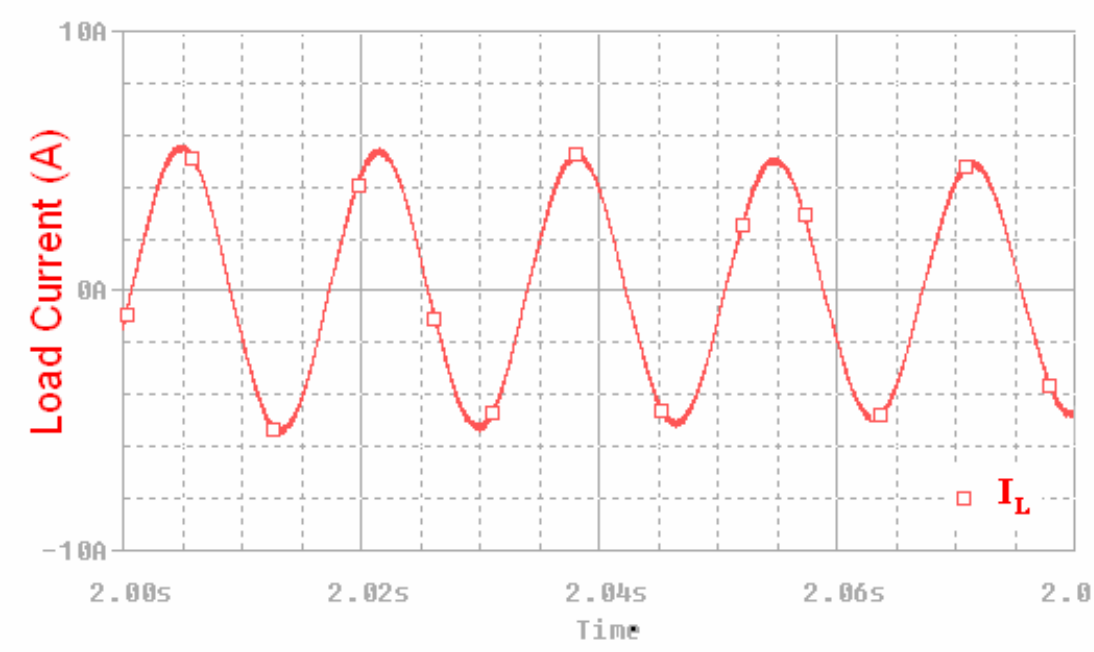


(b)

**Figure 3.16:** Output Waveforms of PWM AC Chopper; **(a)** Load Voltage at D = 0.5, **(b)** Load Current at D = 0.5

### 3.2 Realization of PWM AC Chopper

Figure 3.17 shows the realized AC Chopper. UC3525 is the PWM Generator used. It produces a triangle wave with minimum value of 0.8V and 3.2V oscillating at the frequency depending on $R_1$ and $C_1$. $R_1$ and $C_1$ are selected 5kΩ and 10nF respectively fixing the oscillation frequency to 25 kHz. In open loop configuration the triangle wave was compared to a DC voltage reference derived by a variable resistor $R_V$. Pin number 11 and 14 of the UC3525 PWM generator were summed by two 1 kΩ resistors in order to produce the pulse width modulated signal. This signal is applied to TC428 MosFET driver which uses the input and generates two complementary PWM signals. These signals are applied to the gates of the MosFETs by optical isolation. TLP251 optical couplers were used to produce isolation and to drive the mosfets. Also pulse transformers could be used as gate drive components and isolation.

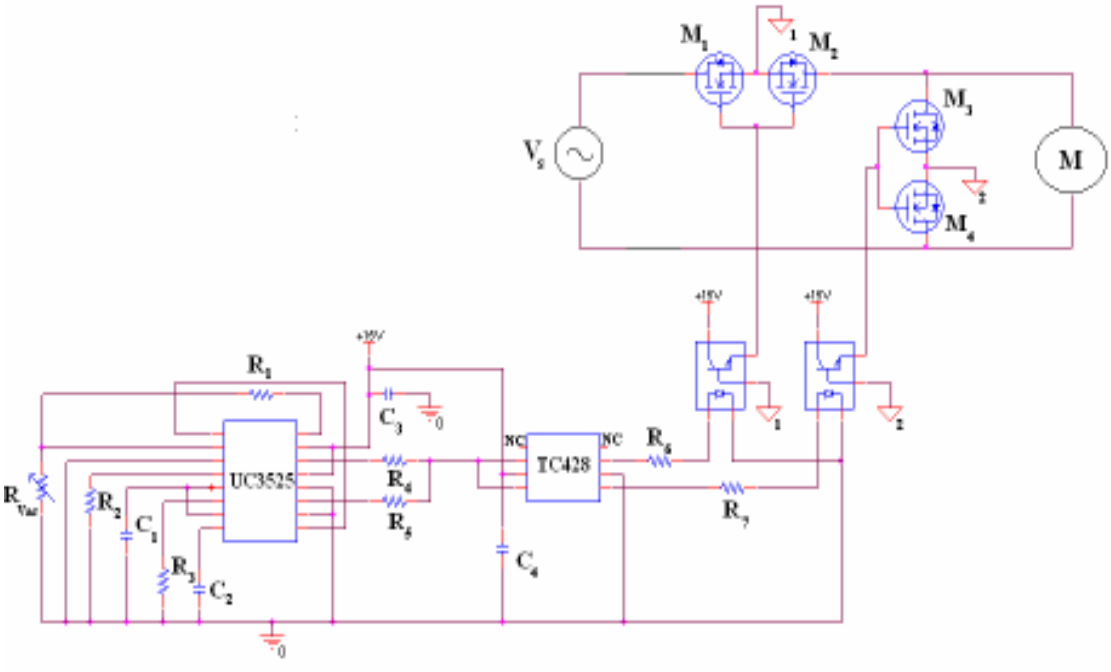


**Figure 3.17:** PWM AC Chopper with Optical Isolation

Figures 3.18 shows the measurement results of inputs to comparator of the PWM generator and the pulse width modulated output of UC3525. The PWM generator UC3523 does not allow the duty cycle ($D$) to be 1 due to its properties. Figure 3.19 shows the MosFETs gate-source signals.

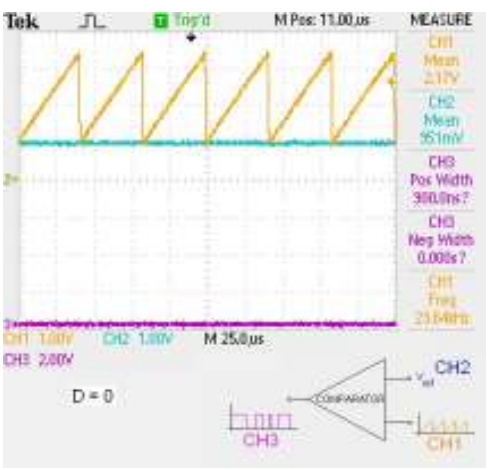


**(a)**

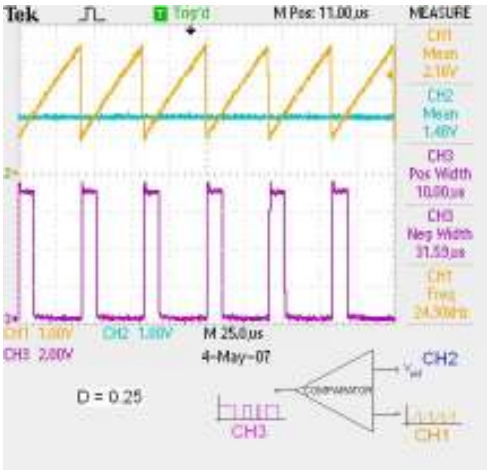


**(b)**

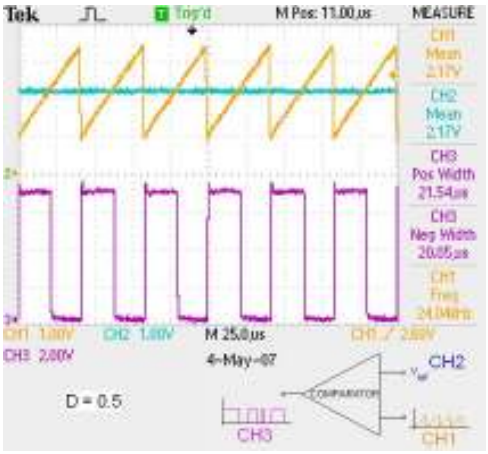


**(c)**

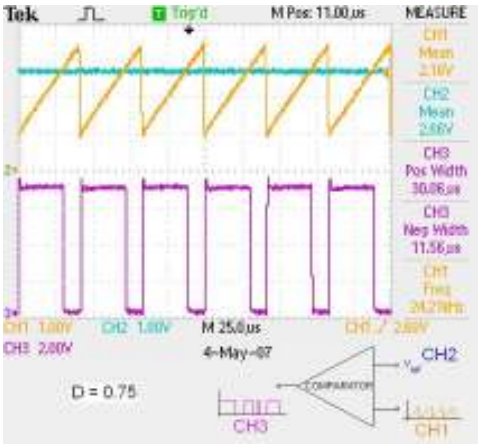


**(d)**

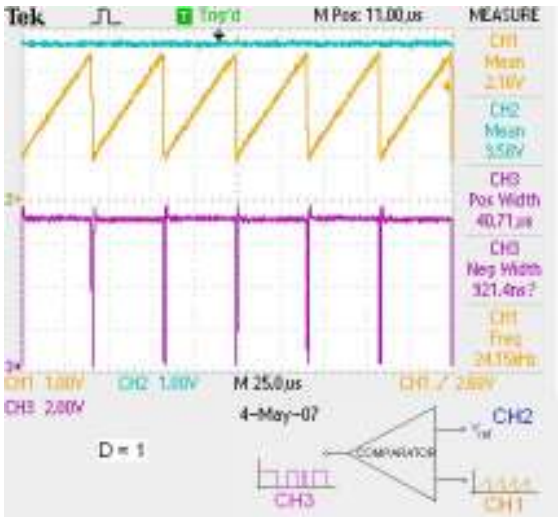


**(e)**

**Figure 3.18:** MosFET Gate-Source Signals for Different Duty Cycles (*D*);
**(a)** D = 0, **(b)** D = 0.25, **(c)** D = 0.5, **(d)** D = 0.75, **(e)** D = 0.99

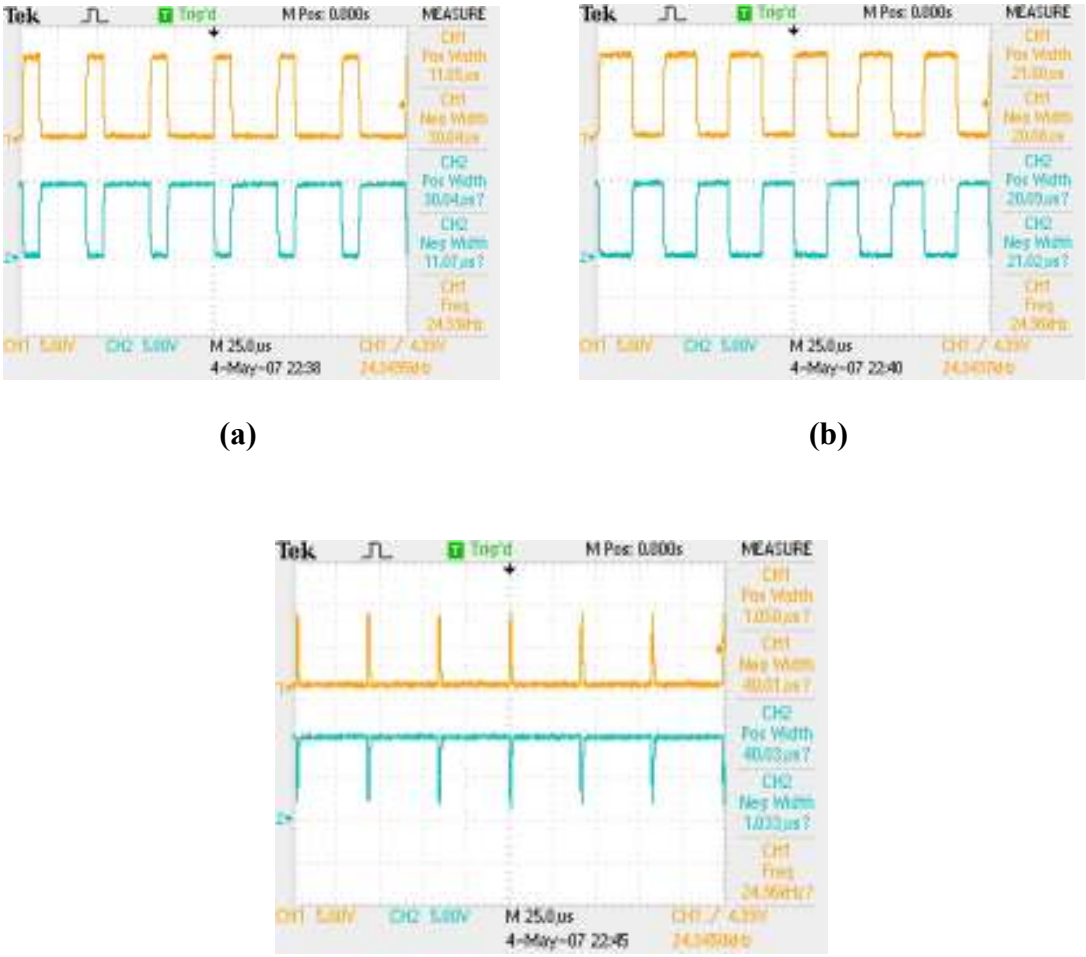


**(a)** **(b)**

**(c)**

**Figure 3.19:** MosFET Gate-Source Signals; (Voltage Division= 5V, Time Division= 25µs); **(a)** D = 0.125 (for channel 1), **(b)** D = 0.5 (for channel 1), **(c)** D = 0.99 (for channel 1)

In these conditions the PWM AC Chopper was not able to work properly on full supply voltage (220VAC, 50Hz). The circuit was capable of working at 110V 50Hz conditions because of the input voltage and current harmonics. These harmonics caused extreme heating and failure of the MosFETs. The experimental results show us that these peak currents in steady state operation can be three times greater than the average value. Figure 3.20 and Figure 3.21 show the simulation and experimental results of these current and voltage harmonics, respectively. An input filter between the supply and PWM AC Chopper is required to eliminate these high frequency harmonics.

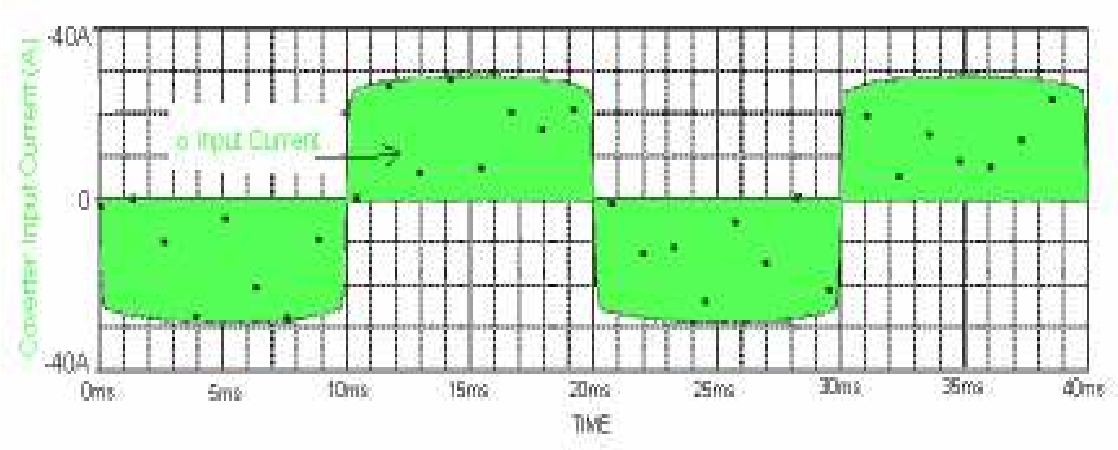


**Figure 3.20:** Simulation Results of Input Current (at 110V, 60Hz)

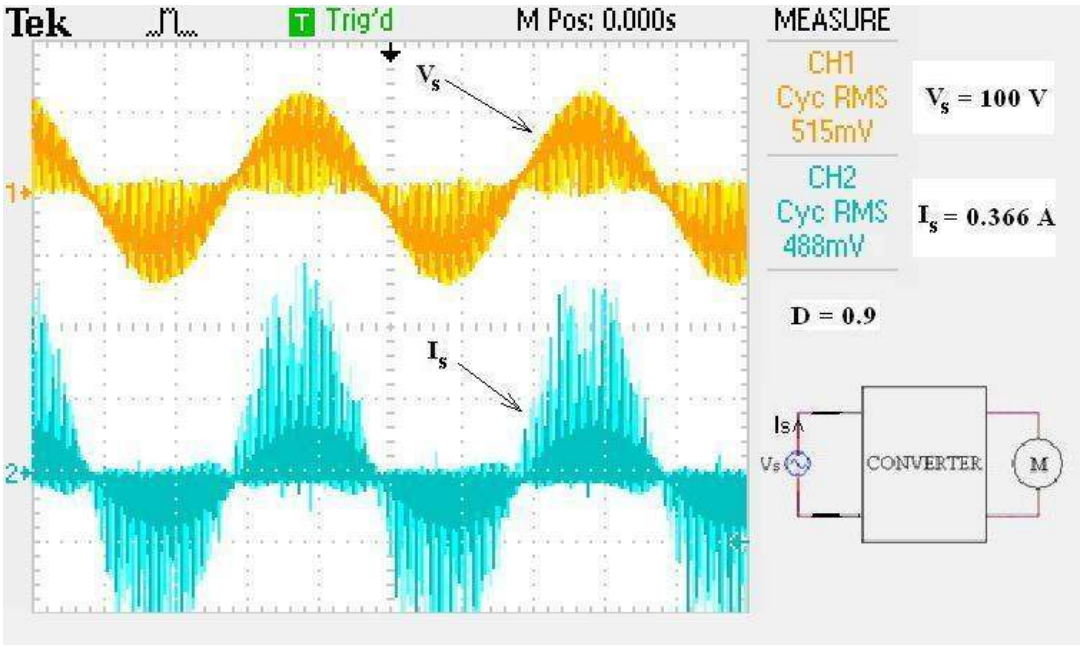


**Figure 3.21:** Experimental Results of Input Voltage ($V_s$) and Input Current ($I_s$) Waveforms (110V, 50Hz, D=0.9, Time Division = 5ms, Voltage Division = 200V, Current Division = 0.75A)

High peak currents occur due to the switching overlaps in very short time intervals. The experimental results in Figure 3.21 show the current peaks reaching two and a half times greater then its nominal values. The worst case for these peaks are seen when the duty cycle is near 1.

## 4. INPUT FILTER DESIGN

In this section the harmonic distortions caused by the switching actions and standards that limit these distortions are discussed. The design of a proper input filter for desired limits is also given in this section.

It is nearly always required that a filter must be added at the power input of a switching converter for improving power quality and interface issues. By attenuating the switching harmonics that are present in the converter input waveform, the input filter allows compliance with regulations that limit conducted electromagnetic interference (EMI). The input filter can also protect the converter and its load from transients that appear in the input voltage, therefore improving the system reliability. [5]

The PWM AC Chopper designed before, injects the pulsating current $I_C$ into the power source $V_S$. The Fourier series of $I_C(t)$ contains harmonics at multiple of the switching frequency $f_S$.

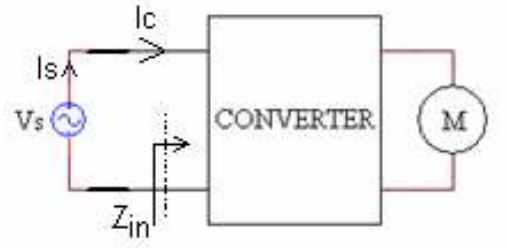


**Figure 4.1:** Simplified Converter Diagram

Equations 2.4 to 2.15 show the derivation of the PWM signal applied to the load in means of Fourier analysis. It can also be seen from these equations that the harmonics depend on Duty Cycle ($D$). The input current $I_s(t)$ and input voltage $V_s(t)$ have similar degrees of harmonics as it is in load voltage. The analysis of load voltage harmonics can lead us to the solution of input current and voltage harmonic reduction.

The Fourier coefficients $a_n$ and $b_n$ are the magnitudes of the harmonic components. $c_n$ gives a resultant coefficient of $a_n$ and $b_n$. The following Figure 4.2 shows the $c_n$ coefficients with respect to the change of $n$ (coefficient numbers) and $D$ (duty cycle).

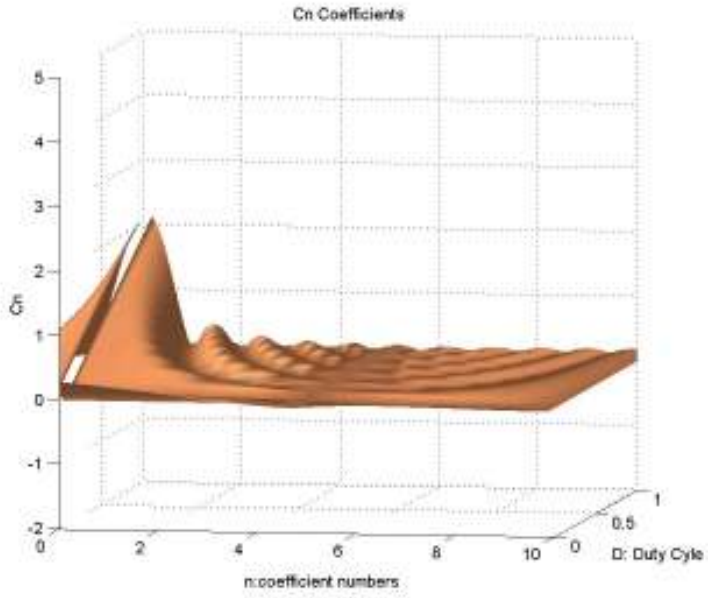


**Figure 4.2:** $c_n$ Coefficients

$C_n$ are important because most of the measurement instrument measure the FFT values according to the $c_n$ coefficient values. The following figures show the experimental FFT results of the realized PWM AC Chopper compare with there analytic results derived by MATHLAB using Equation 2.10. The results do match in some parts but it is difficult to compare them. The main reason for this difficulty is the FFT aliases.

The highest frequency that any real-time digitalizing oscilloscope can measure with out errors is one-half of the sample rate. This frequency is called the Nyquist frequency. Problems occur when the oscilloscope acquires a time-domain waveform containing frequency components that are greater than the Nyquist frequency. The frequency components that are above the Nyquist frequency are under sampled, appearing as lower frequency components that “fold back” around the Nyquist frequency. These incorrect components are called aliases. [8]

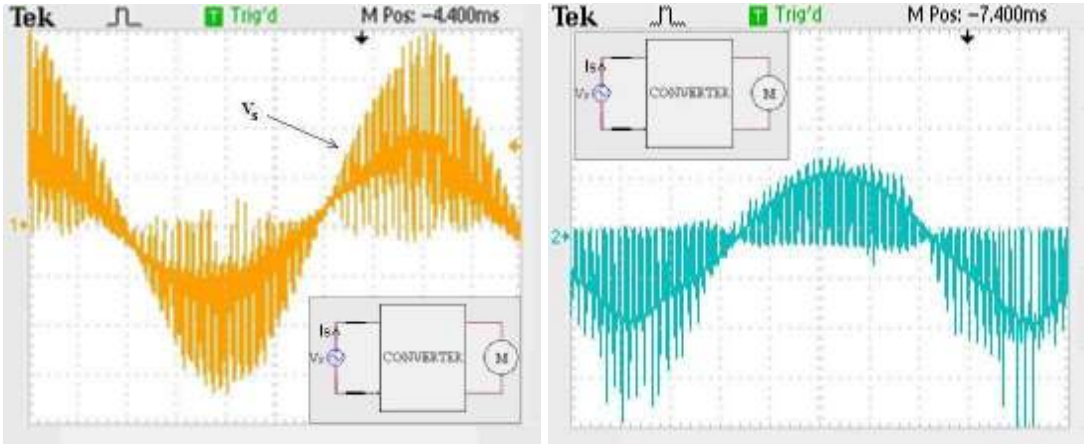


**(a)** **(b)**

**Figure 4.3:** Input Wave forms at 110V, 50Hz, D ≅ 0.9; **(a)** Input Voltage (Voltage Division = 100V, Time Division =2.5ms), **(b)** Input Current (Current Division = 0.75A, Time Division = 2.5ms)

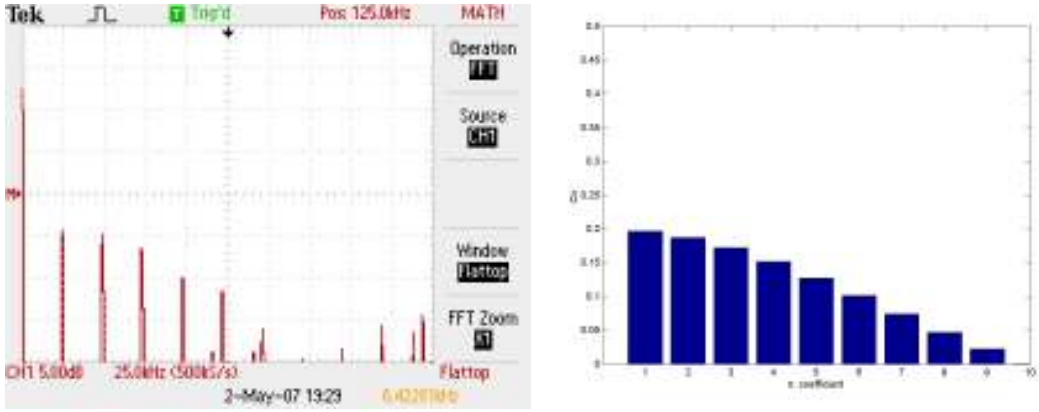


**(a)** **(b)**

**Figure 4.4** FFT of Waveforms in Figure 4.6 (110V, 50Hz, D ≅ 0.9); **(a)** Experimental FFT of Input Voltage (Time Division = 25 kHz), **(b)** Analytic Results of FFT (x axis: n = 1 is the fundamental component at 25 kHz, y axis: magnitude values of $c_n$ derived from equation 2.10)

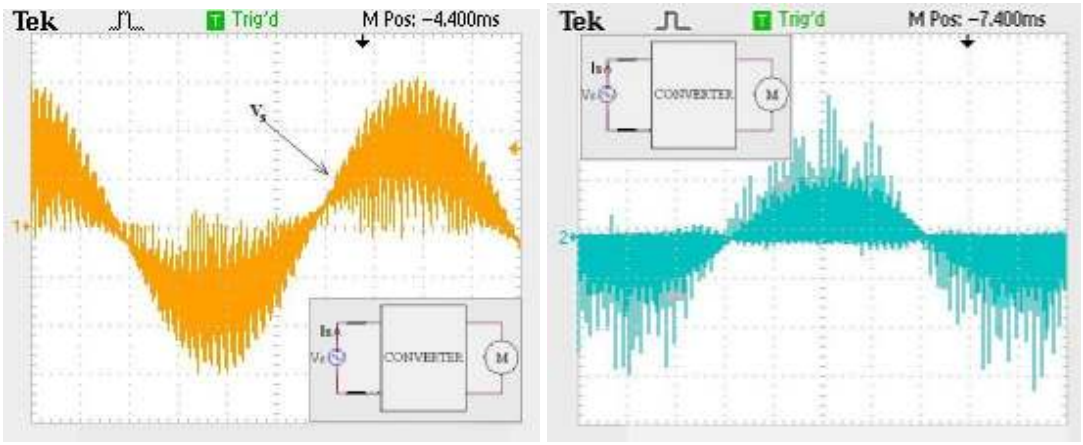


**(a)** **(b)**

**Figure 4.5:** Input Wave forms at 110V, 50Hz, D ≅ 0.75;
**(a)** Input Voltage (Voltage Division = 100V, Time Division =2.5ms), **(b)** Input Current (Current Division = 0.75A, Time Division = 2.5ms)

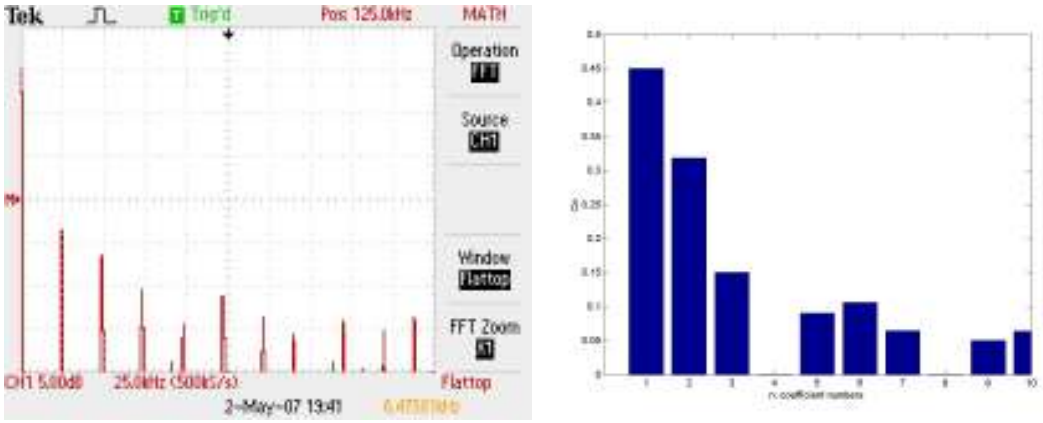


**(a)** **(b)**

**Figure 4.6:** FFT of Waveforms in Figure 4.8 (110V, 50Hz, D ≅ 0.75);
**(a)** Experimental FFT of Input Voltage (Time Division = 25 kHz), **(b)** Analytic Results of FFT (x axis: n = 1 is the fundamental component at 25 kHz, y axis: magnitude values of $c_n$ derived from equation 2.10)

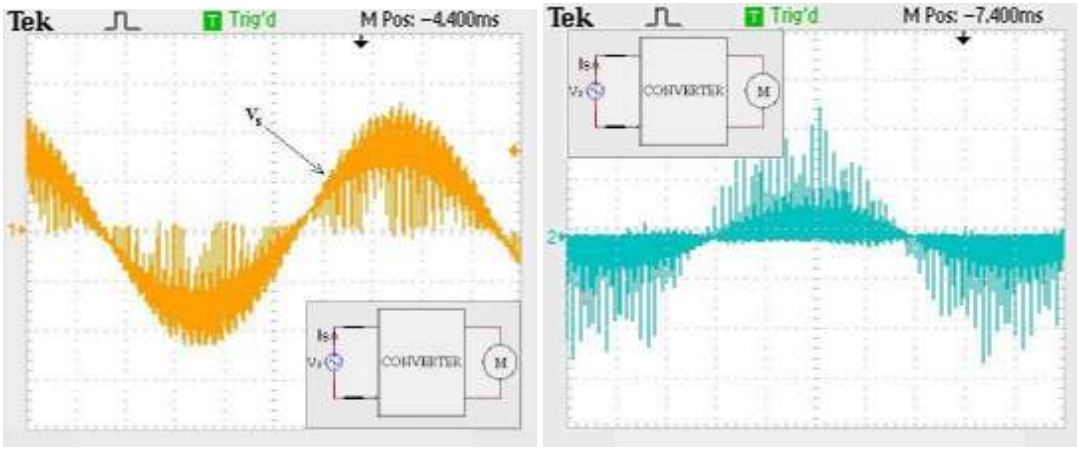


**(a)** **(b)**

**Figure 4.7:** Input Wave forms at 110V, 50Hz, D ≅ 0.5;
**(a)** Input Voltage (Voltage Division = 100V, Time Division =2.5ms), **(b)** Input Current (Current Division = 0.75A, Time Division = 2.5ms)

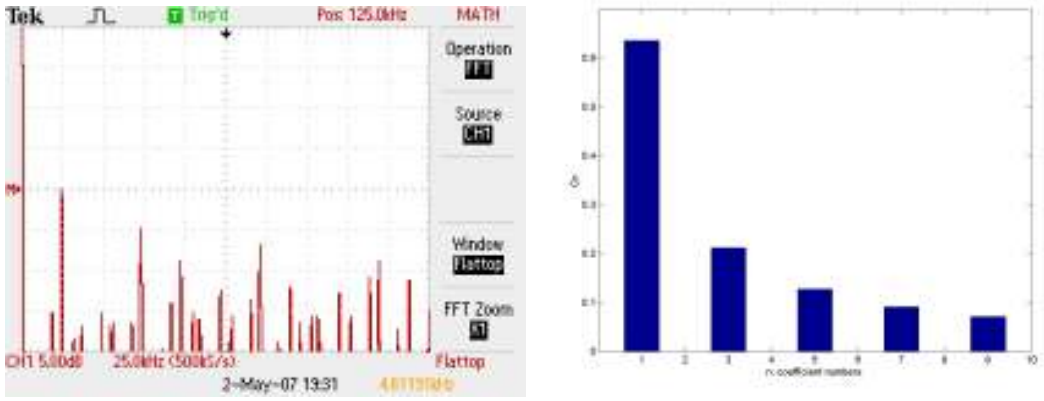


**(a)** **(b)**

**Figure 4.8:** FFT of Waveforms in Figure 4.10 (110V, 50Hz, D ≅ 0.5);
**(a)** Experimental FFT of Input Voltage (Time Division = 25 kHz), **(b)** Analytic Results of FFT (x axis: n = 1 is the fundamental component at 25 kHz, y axis: magnitude values of $c_n$ derived from equation 2.10)

It is seen that the first harmonic starts at 25 kHz which is the switching frequency. Multiples of this harmonic, change in magnitude depending on the duty cycle ($D$). The fundamental component is at 50 Hz which is the supply voltage frequency. It can be seen that the first harmonic appears in a very high frequency compared with the 50Hz fundamental component. These high switching harmonics cause two main problems. The first one is, high frequency switching causes electromagnetic disturbances effecting nearby electronic equipment and the secondly it draws

harmonic currents form the power supply decreasing the power quality. International standards have been developed in order to bring some limits to electromagnetic compatibility (EMC) and power quality issues [9].

### 4.1 Standards for Harmonic Distortions

Standards developed for this application is given in EN 55014 and IEC 61000-3-2.

**EN 55014:** European limits and methods of measurement of radio disturbance characteristics of household appliances and power tools.

According to En 55014 Electromagnetic Compatibility (EMC) measurement requires use of the Line Impedance Stabilization Network (LISN). The LISN operates as a filter between the line and test board, providing clean energy to the system under test. It collects all the emissions coming from the test (>9kHz) and sends the noise to the EMC analyzer. See figure 4.9 for configuration of the system.

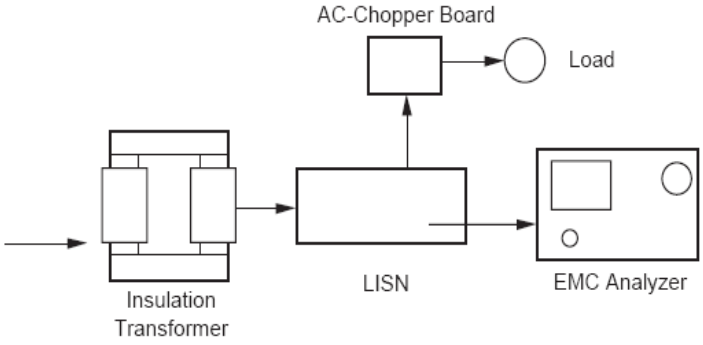


**Figure 4.9:** EMC Measurement Schematic [10]

**Table 4.1:** AC Chopper EMC Limits [10]

| Description(1) | Limit Line | Frequency Range(2) |
|---|---|---|
| EN55014 | Conducted <700W, Motors, Quasi-peak | 150kHz to 30MHz |
| EN55014 | Conducted <700W, Motors, Average | 150kHz to 30MHz |

1. EMC AC chopper measurement at 20kHz switching frequency (CISPR-14), per EN55014 standard.
2. Instrument used: E7400 Agilent Technology

Due to the absence of the necessary measurement equipment, the measurement technique given above was not to be applied in this work.

**IEC 61000-3-2**: Electromagnetic Compatibility limits of harmonic current emissions for equipment current less than 16 A per phase.

This standard, gives the limits of input current harmonics under specified conditions. According to class specifications given in IEC 61000-3-2, the PWM AC Chopper fits to class D. The limits given according to this standard are shown in Table 4.2.

**Table 4.2:** Harmonic Standards According to IEC 61000-3-2 [10]

| **Harmonic Number (n)** | **Maximum Harmonic Current Allowed for 200W** | **Maximum Harmonic Current** |
|---|---|---|
| 3 | 680 mA | 2.30 A |
| 5 | 380 mA | 1.14 A |
| 7 | 200 mA | 0.77 A |
| 9 | 100 mA | 0.40 A |
| 11 | 70 mA | 0.33 A |
| $13 \leq n \leq 39$ | 770/n mA | 0.15x15/n A |

### 4.2 Input Filter Design

The addition of an input filter affects the dynamics of the power electronic converters, often in a manner that degrades the regulator performance. The input filter affects all transfer functions of converter. More over the influence of this input filter on these transfer functions can be quite severe [5].

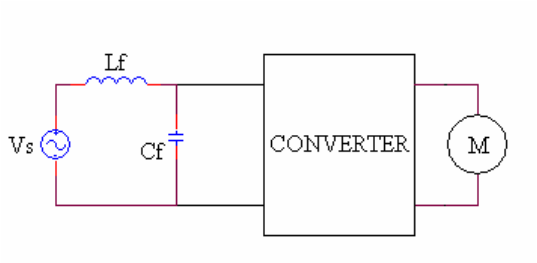


**Figure 4.10:** Undamped LC Input Filter

Figure 4.10 shows the structure of a simple LC filter. The corner frequency of this filter was set to about 10 kHz, using a 300 µH inductance and 1µF capacitor. The following figure shows the bode diagram of the LC filter.

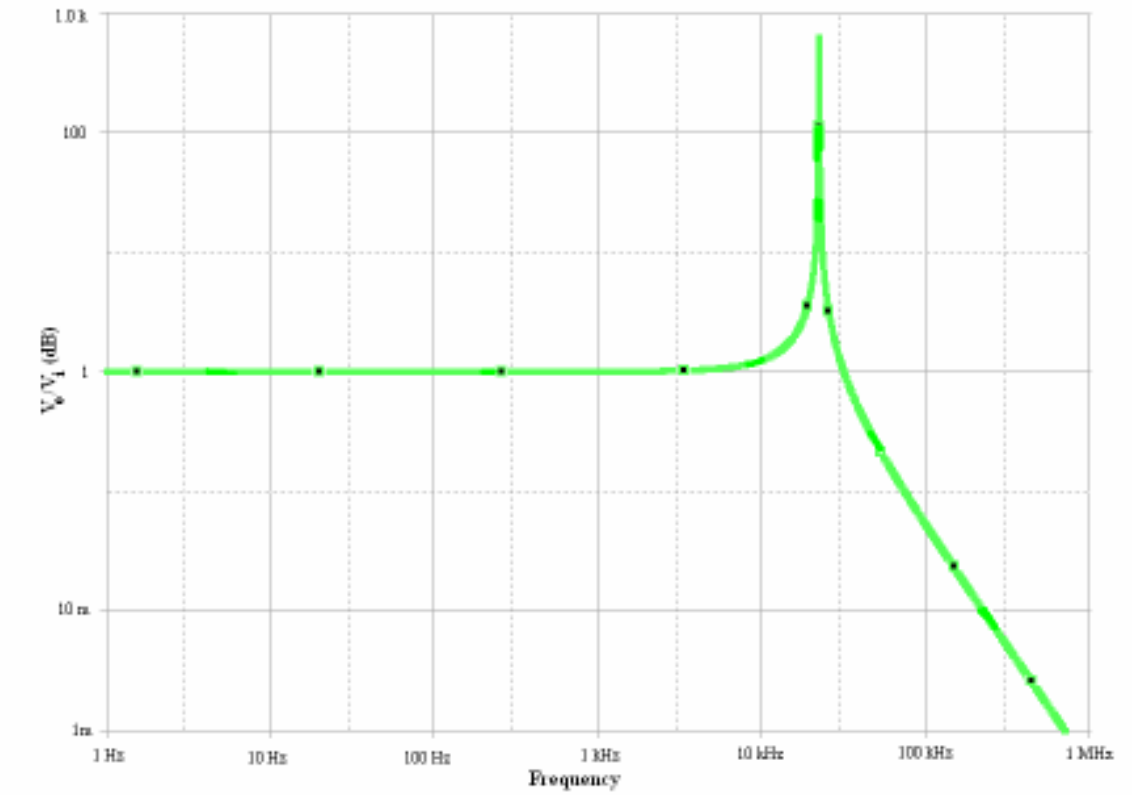


**Figure 4.11:** Frequency Response of LC filter in Figure 4.10

The bode diagram shows an asymptotic peak occurring near the corner frequency causing the gain of the filter to go to infinity. This rise would cause extreme current peaks which would make the system worse than it was before.

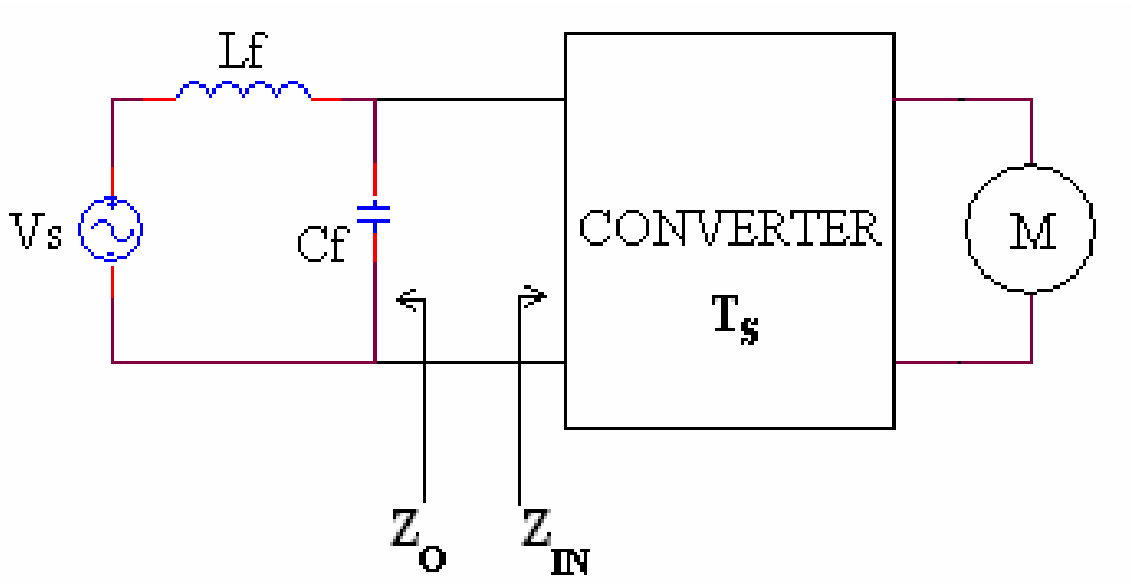


**Figure 4.12:** LC Input Filter

From figure 4.12 $Z_o$, is the output impedance of the input filter, $Z_{IN}$ is the input impedance of the converter and $T_s$ is the transfer function of the converter. The affect of the input filter to the transfer function can be represented by Middlebrook's extra element theorem [11]

$$T_S^{'}(s) = T_s(s)\left[\frac{\left(1+\frac{Z_O(s)}{Z_{IN}(s)}\right)}{\left(1+\frac{Z_O(s)}{Z_{ID}(s)}\right)}\right] \tag{4.1}$$

where $Z_{ID}$ is the open loop input impedance of the converter an $T_S^{'}$ is the modified transfer function with input filter. It can be seen from equation 4.1 that the transfer function does not significantly modify the transfer function provided that [11],

$$\begin{aligned} &\|Z_O\| \ll \|Z_{IN}\| \\ &and \\ &\|Z_o\| \ll \|Z_{ID}\| \end{aligned} \tag{4.2}$$

These inequalities limit the maximum allowable output impedance of the input filter and constitute useful design criteria [11].

The equations 4.1 and 4.2 explain why the input filters lead to converter oscillations. The output impedance $Z_O(s)$ tends to infinity at frequencies near corner frequency $f_0$ [11].

$$f_0 = \frac{1}{2\pi\sqrt{L_f C_f}} \tag{4.3}$$

Figure 4.13 show an implementation of a damping factor to the converter input. The component values of the damped filter are calculated from [11]. For this filter design let define the quantity $k$ as the ratio of the blocking capacitor to filter capacitor

$$k = \frac{C_b}{C_f} \tag{4.4}$$

For optimum design, the peak output impedance occurs at the frequency;

$$f_m = f_f \sqrt{\frac{2}{2+k}} \tag{4.5}$$

The value of peak output impedance for optimum design is;

$$\|Z_o\|_{opt} = R_{of} \sqrt{\frac{2(2+k)}{k}} \tag{4.6}$$

The value of optimum resistance that leads to optimum damping is described by.

$$Q_{opt} = \frac{R_f}{R_{of}} = \sqrt{\frac{(2+k)(4+3k)}{2k^2(4+k)}} \tag{4.7}$$

$R_f$ and $R_{of}$ are the characteristic impedances of the input filter. [11]

$L_f$ and $C_f$ where selected to be 300 µH and 1µF, respectively for 10 kHz corner frequency. $C_b$ was selected 0.1 µF. From these three values the optimum value for damping resistance is calculated to be 120Ω.

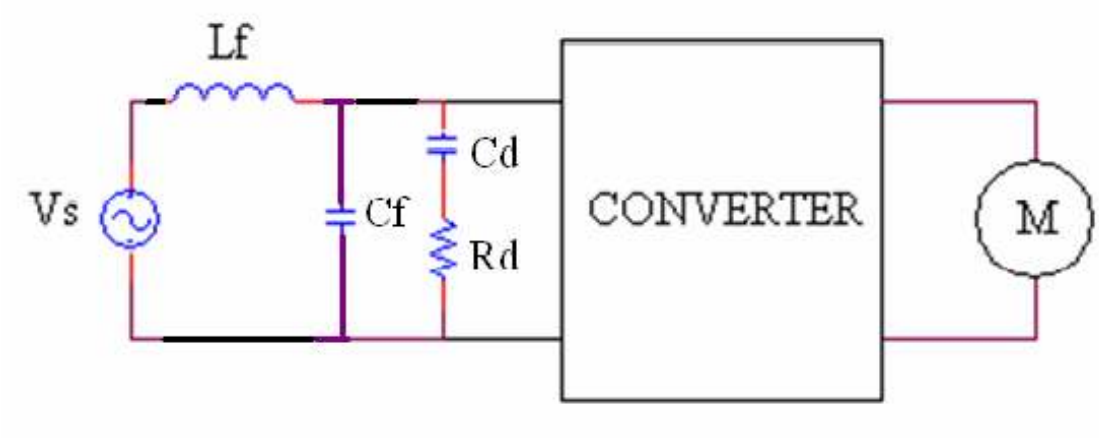


**Figure 4.13:** Damped Input Filter

$L_f$, $C_f$, $C_d$ and $R_d$ have the following values 300µH, 1µF, 0.1µF, 120Ω respectively. The Bode diagram of the designed input filter is now damped as shown below.

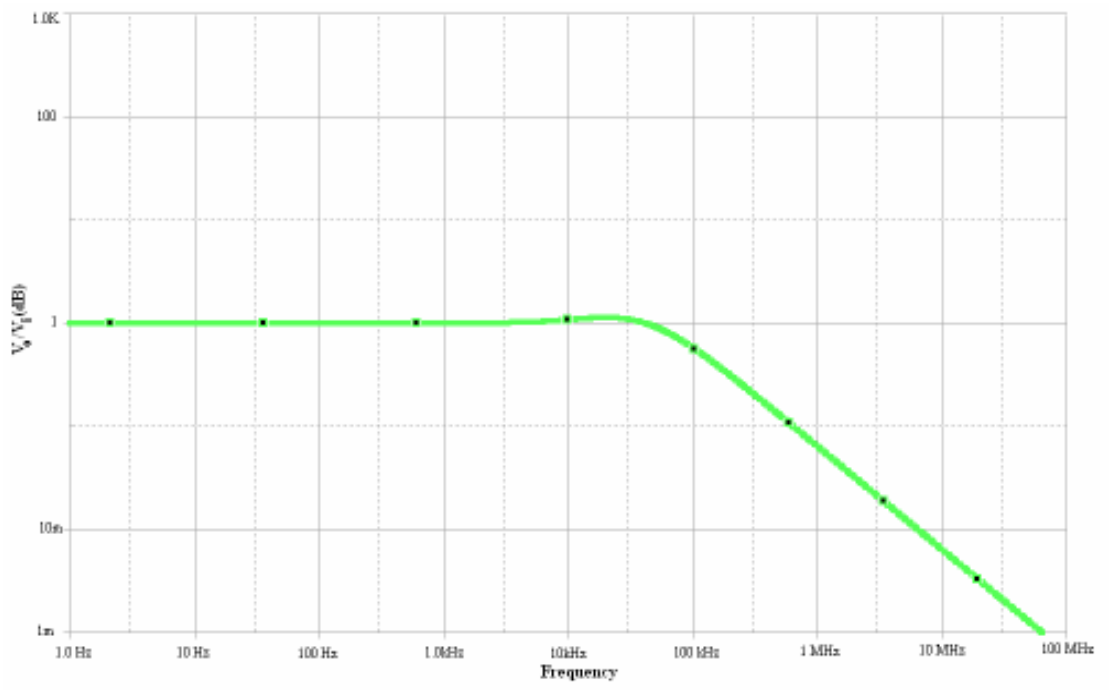


**Figure 4.14:** Frequency Response of Damped Input Filter

Simulation results that, the use of damped filter reduces the current peaks shown in Figure 3.20. The following figure shows the reduced current peaks of the converter input current.

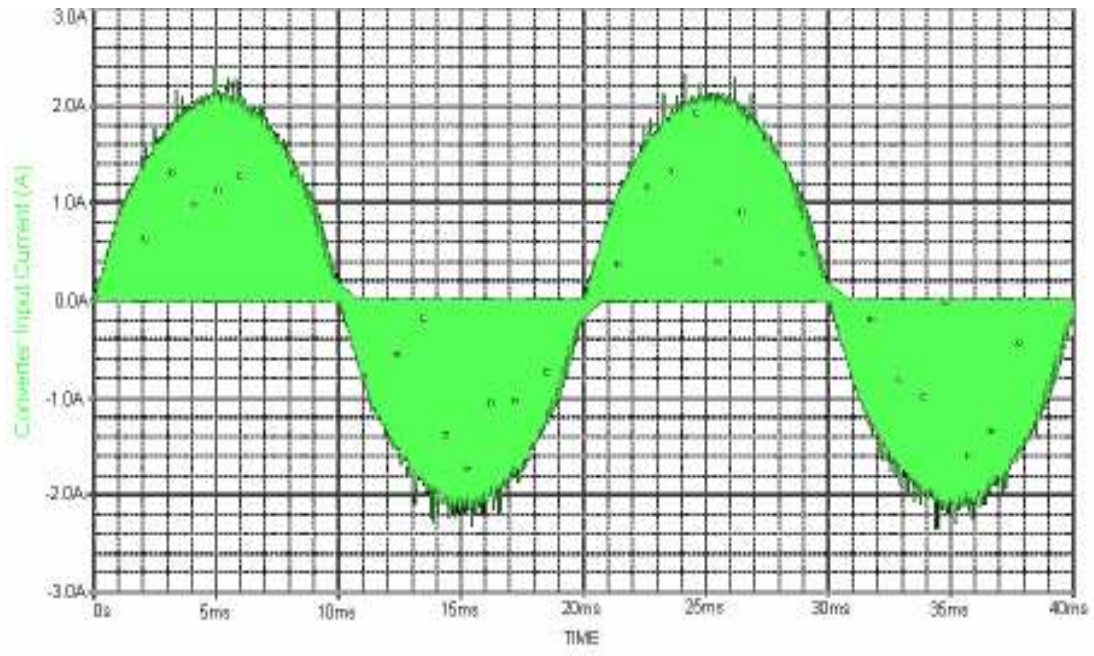


**Figure 4.15:** Simulation Results of Converter Input Current with Damped Filter (Simulated at 110V, 60Hz)

Figure 4.15 shows that most of the current peaks caused by the switching action in the converter have been reduced by a damped input filter. The following figures show the experimental results of the input voltage, input current and the converter input current with reduced current peaks. The results where taken at full supply voltage at 220V at 50Hz.

Figure 4.16 and 4.17 shows the input current, input voltage and converter input current for duty cycles D = 0.75 and D = 0.5, respectively in time domain. These results, which are obtained by TDS2000B series Digital Storage Oscilloscope, show that the filter designed eliminates the high frequency harmonics.

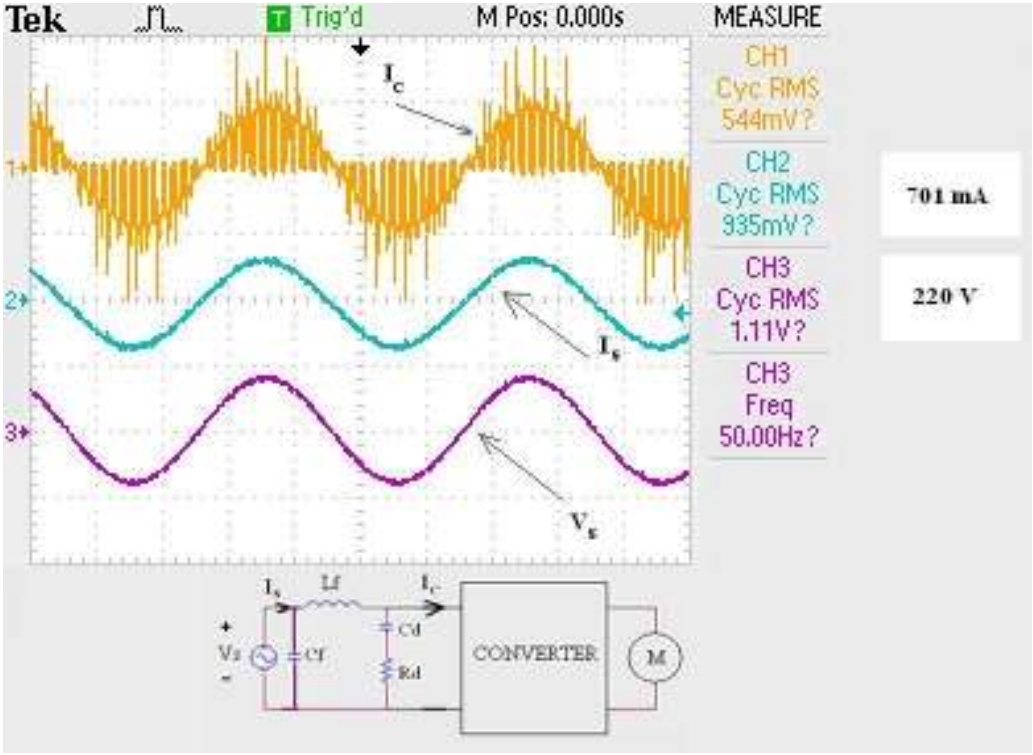


**Figure 4.16:** Input Current, Input Voltage and Converter Input Current
(D = 0.75, Time Division = 5ms, Voltage Division = 400V, Current Division = 1.5A)

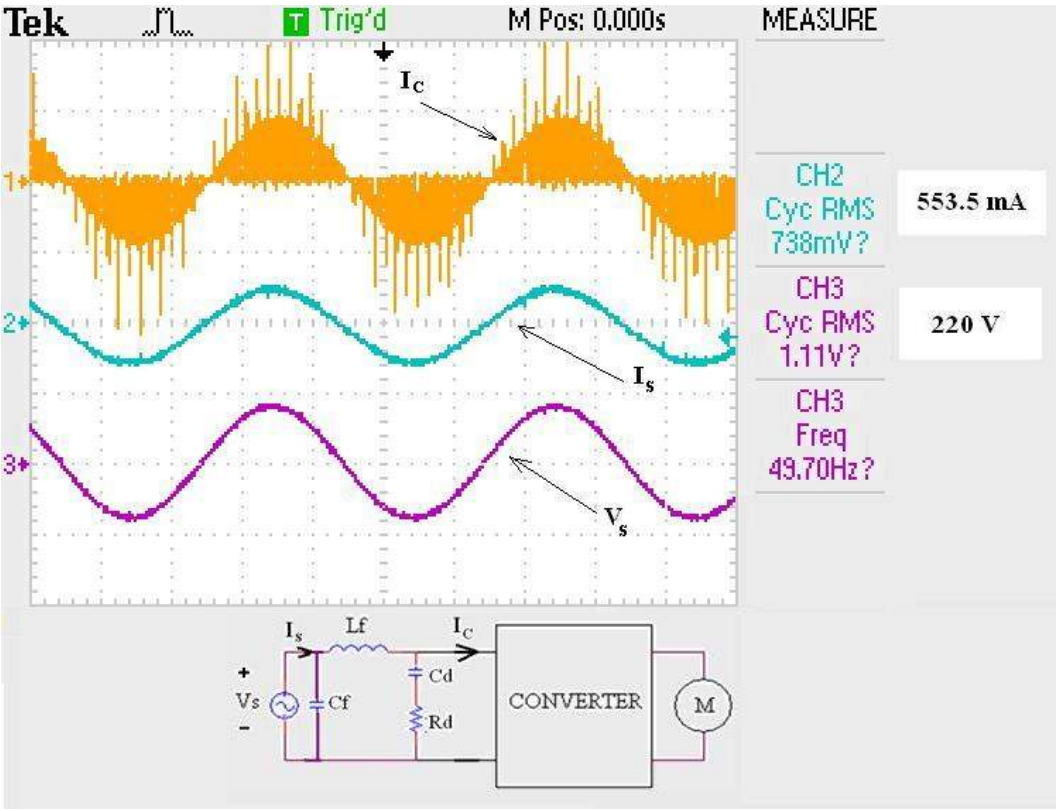


**Figure 4.17:** Input Current, Input Voltage and Converter Input Current (D = 0.5, Time Division = 5ms, Voltage Division = 400V, Current Division = 1.5A)

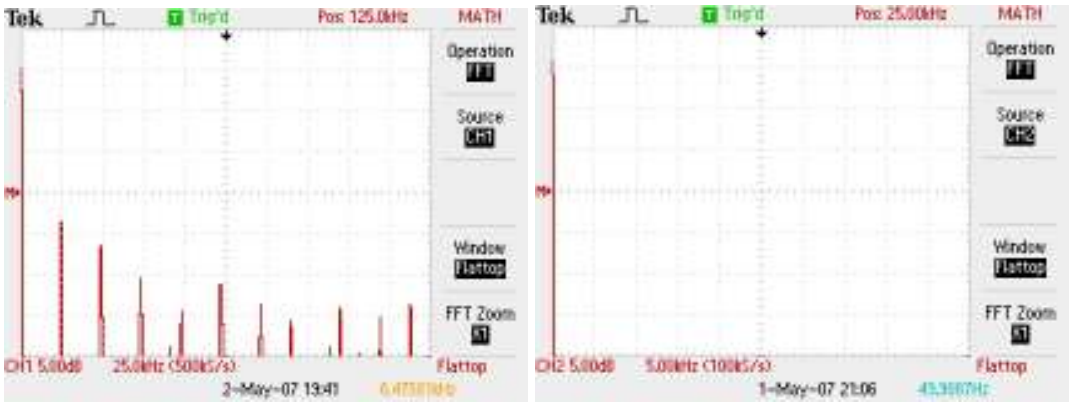


**(a)** **(b)**

**Figure 4.18:** Experimental Analysis of FFT for Input Current Harmonics (D = 0.75); **(a)**Unfiltered FFT of Input Current (Time Division = 25 kHz/div, Supply Voltage = 110V, Supply Frequency = 50Hz), **(b)** FFT of Input Current with Damped Input Filter (Time Division = 5 kHz/div, Supply Voltage = 220V, Supply Frequency = 50Hz)

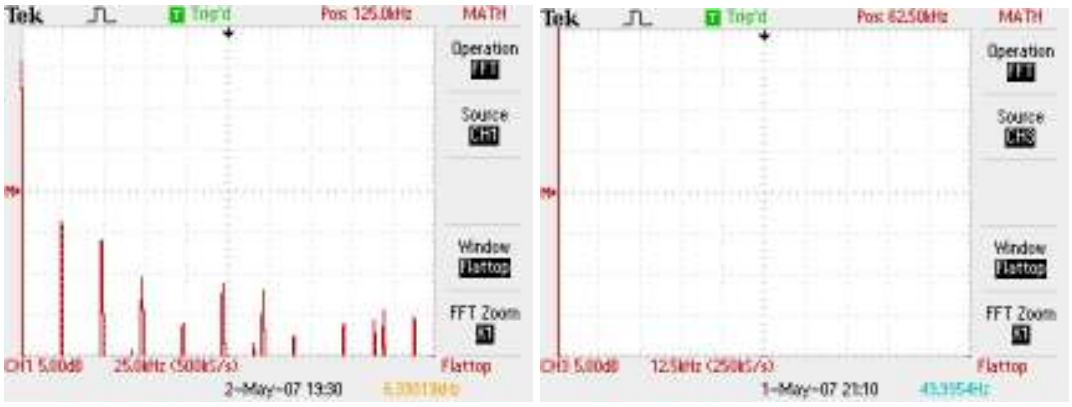


**(a)** **(b)**

**Figure 4.19:** Experimental Analysis of FFT for Input Voltage Harmonics (D = 0.75); **(a)**Unfiltered FFT of Input Voltage (Time Division = 25 kHz/div, Supply Voltage = 110V, Supply Frequency = 50Hz), **(b)** FFT of Input Voltage with Damped Input Filter (Time Division = 12.5 kHz/div, Supply Voltage = 220V, Supply Frequency = 50Hz)

Figure 4.18 and 4.19 show the harmonic eliminations in the input current and voltage, respectively in frequency domain. These experimental results are obtained with TDS2000B series Digital Storage Oscilloscope in FFT mode.

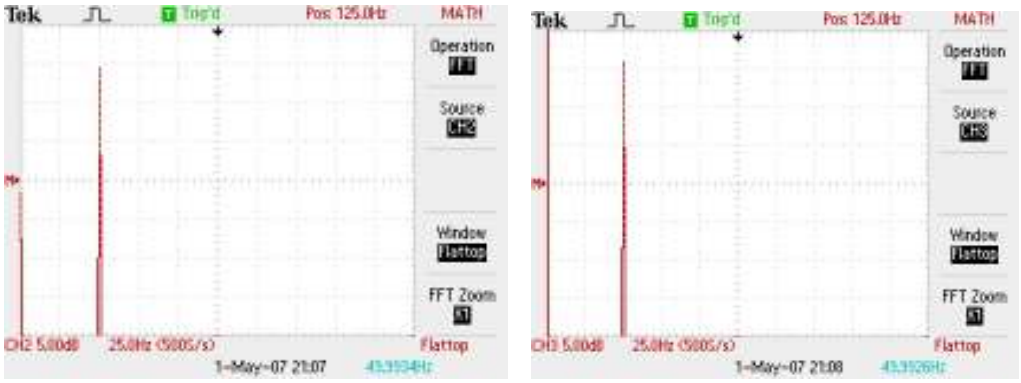


(a) (b)

**Figure 4.20:** Experimental Results Filter Input Current and Input Voltage. Figure Shows no Low Frequency Harmonics after 50 Hz Fundamental Component (D = 0.75); **(a)** FFT of Input Current with Damped Input Filter Showing 50Hz Fundamental Component (Time Division = 25 Hz/div, Supply Voltage = 220V, Supply Frequency = 50Hz), **(b)** FFT of Input Voltage with Damped Input Filter Showing 50Hz Fundamental Component (Time Division = 25 Hz/div, Supply Voltage = 220V, Supply Frequency = 50Hz)

### 4.3 Experimental Results of the PWM AC Chopper with Damped Input Filter

We have seen the damped filter and its results to the input current and voltage in the previous section. With these results the overall circuit configuration is shown below in Figure 4.21. According to this design, this is also the final form of the PWM AC Chopper; we have made experimental tests on the reliability of the system. These measurement results can be seen in Table 4.3.

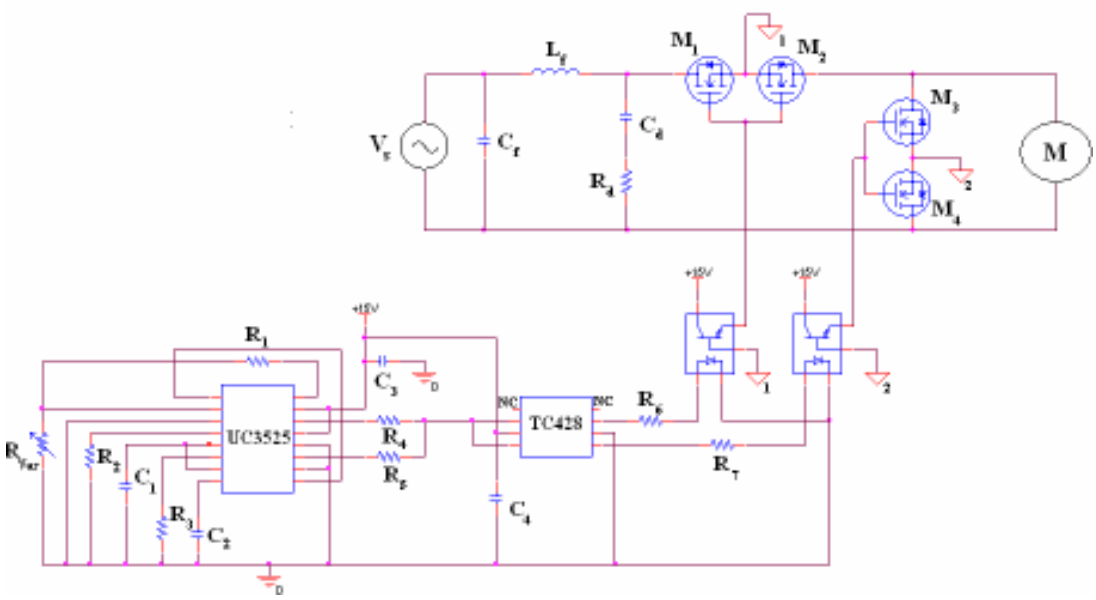


**Figure 4.21:** Realized PWM AC Chopper with Damped Input Filter

Table 4.3 shows the change of load voltage ($V_{Lrms}$), supply current ($I_{in}$), power driven from the utility ($P_{in}$), Power delivered to the motor ($P_{out}$), power consumed by the converter ($P_c$) and the change of speed with reference to $V_{ref}$. $V_{ref}$ is the PWM generator reference signal (control input) which varies the duty cycle of the MosFET gate signals. Figure 4.22 shows the power delivered to the load from the utility and the power consumed by the converter, according to table 4.3. Figures 4.23 and 4.24 show the output characteristic of the converter.

**Table 4.3:** Measurement Results of complete PWM AC Chopper

| Duty Cycle (*D*) | $V_{L,rms}$ (V) | $I_{in}$ (A) | $P_{in}$ (W) | $P_{out}$ (W) | Speed (rpm) | $P_c$ (W) | Efficiency (η) |
|---|---|---|---|---|---|---|---|
| 1 | 220,00 | 0,931 | 202,50 | 198,50 | 2699 | 4,00 | 0,980247 |
| 0,93 | 200,00 | 0,890 | 195,00 | 180,00 | 2639,00 | 15,00 | 0,923077 |
| 0,80 | 180,00 | 0,758 | 169,50 | 152,20 | 2450,00 | 17,30 | 0,897935 |
| 0,67 | 160,00 | 0,659 | 146,90 | 126,20 | 2080,00 | 20,70 | 0,859088 |
| 0,58 | 140,00 | 0,516 | 114,70 | 92,00 | 1536,00 | 22,70 | 0,802092 |
| 0,45 | 120,00 | 0,339 | 75,00 | 54,00 | 1030,00 | 21,00 | 0,72 |
| 0,35 | 100,00 | 0,216 | 46,30 | 24,70 | 683,00 | 21,60 | 0,533477 |
| 0,25 | 80,00 | 0,147 | 28,80 | 9,50 | 421,00 | 19,30 | 0,329861 |
| 0,18 | 60,00 | 0,114 | 18,50 | 2,40 | 214,00 | 16,10 | 0,12973 |
| 0,1 | 40,00 | 0,106 | 12,90 | 0,25 | 60,00 | 12,65 | 0,01938 |
| 0,05 | 20,00 | 0,104 | 12,30 | 0,04 | 0,00 | 12,26 | 0,003252 |
| 0 | 0,00 | 0,102 | 12,30 | 0,01 | 0,00 | 12,29 | 0,000813 |

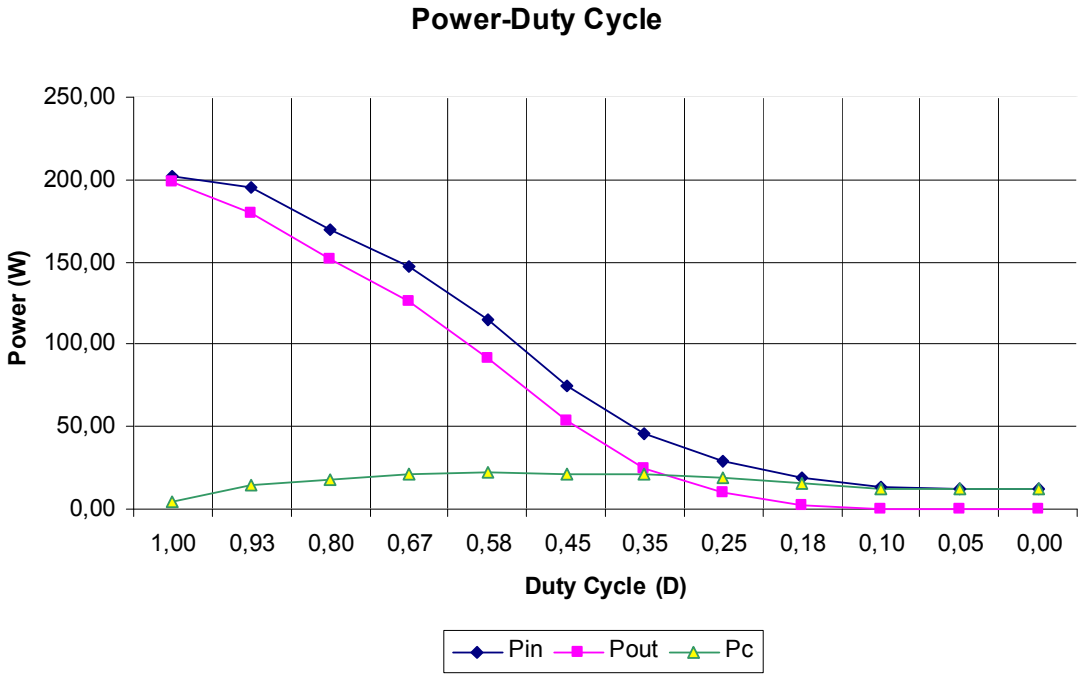


**Figure 4.22:** Input, Output Powers and Losses of the Converter with Respect to Duty Cycle (*D*)

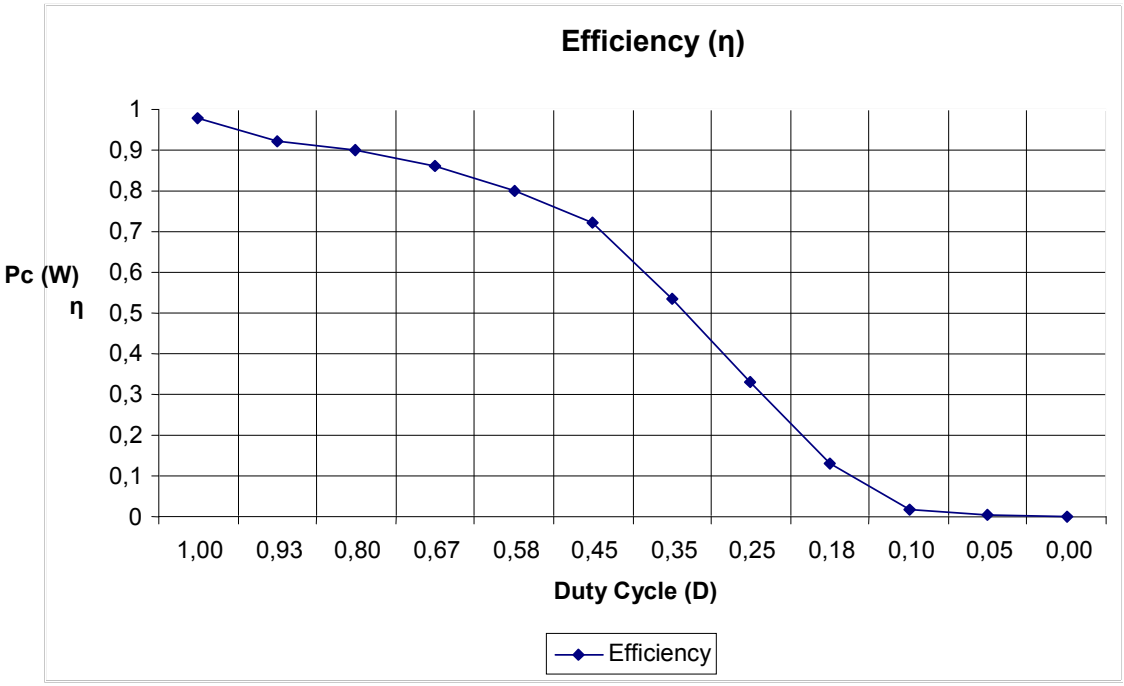


**Figure 4.23:** Efficiency of the PWM AC Chopper for Different Duty Cycles

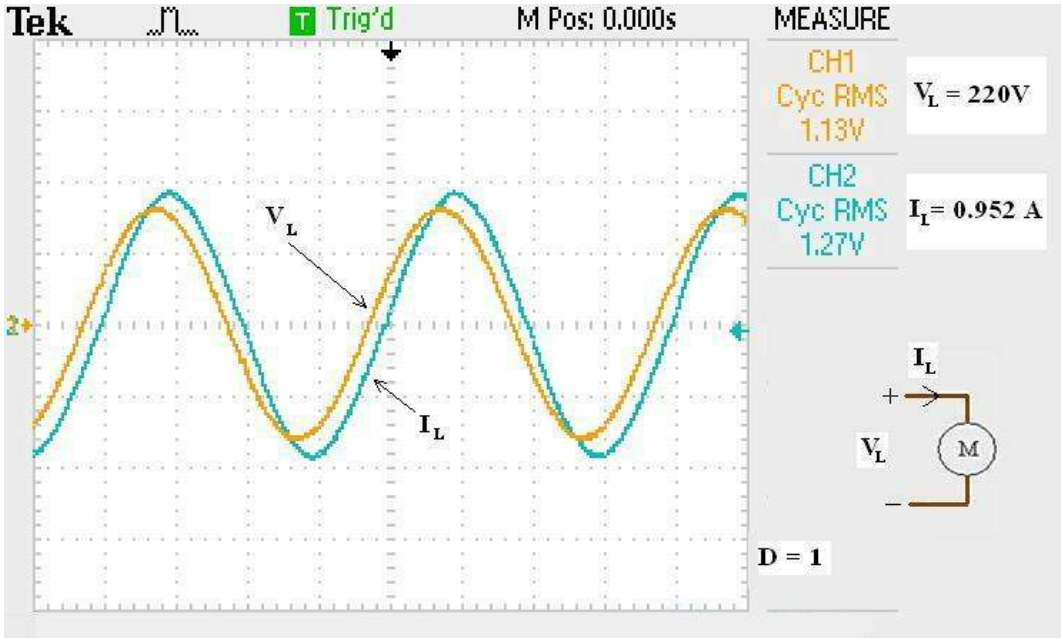


**Figure 4.24:** Output Voltage and Output Current
(D = 1, Time Division = 5ms, Voltage Division = 200V, Current Division = 0.75A)

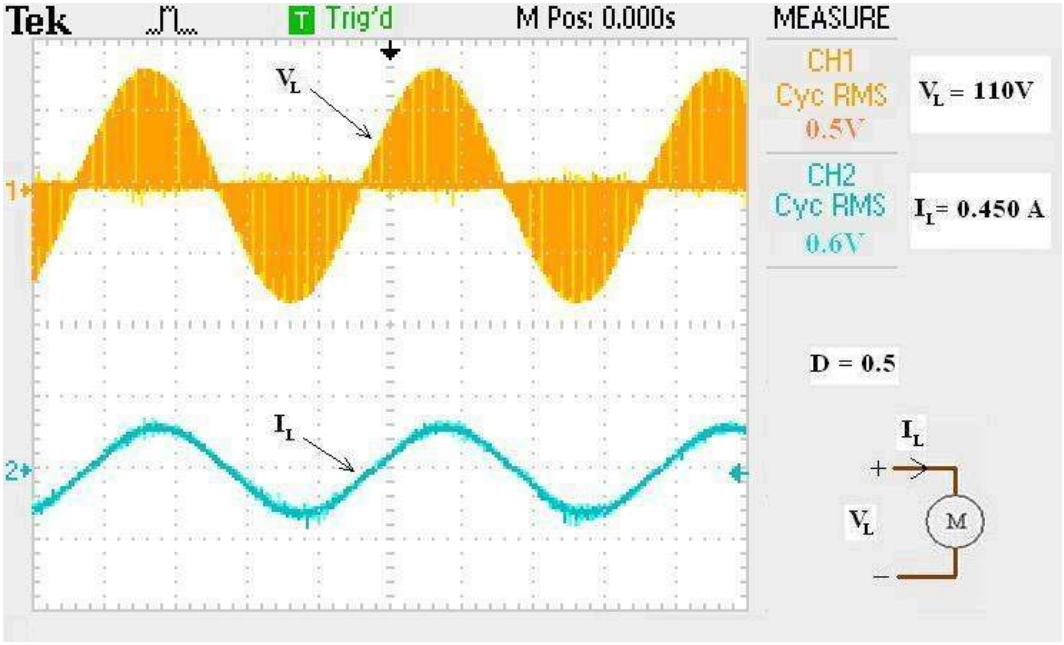


**Figure 4.25:** Output Voltage and Output Current
(D = 0.5, Time Division = 5ms, Voltage Division = 200V, Current Division = 0.75A)

As said before the AC Chopper level must be isolated from driving network. The realized circuit shown in Figure 4.21 is isolated using opto-couplers. The opto-couplers work both well in isolation and signal transfer but these isolated drivers need two isolated power supplies. This causes complexity in the total circuit. A secondary circuit was developed using a pulse transformer to isolate the two stages instead of opto-couplers. The advantage of a pulse transformer is that there is no need for two extra isolated power supplies. The pulse transformer has an important disadvantage in which the designer must keep in mind. A transformer is not capable of transferring DC signals. Therefore the drive network must be designed to work in the duty cycle range between 0.1 and 0.9. In any case of a duty cycle of 0 or 1 would force to open both of the bi-directional switches at the same time. In Figure 4.26 the realized PWM AC Chopper isolated with pulse transformer is given.

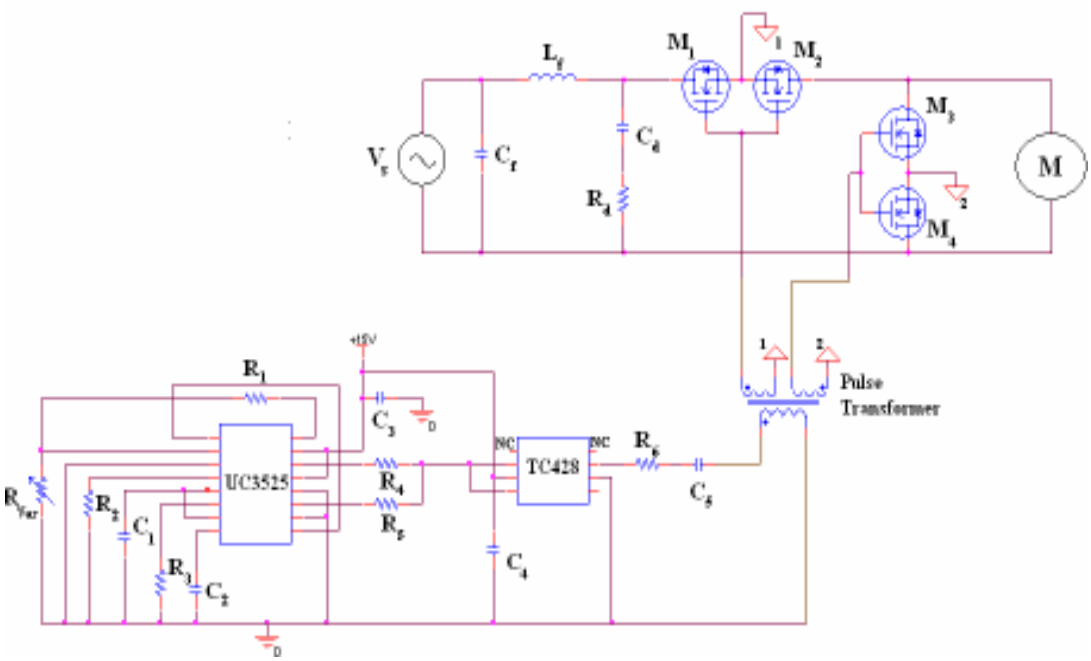


**Figure 4.26:** Realized PWM AC Chopper with Pulse Transformer Isolation

The circuit shown in Figure 4.26 has the same filter designed for the chopper shown in Figure 4.21. Also the driving circuitry is the same. The following figures show the output voltage, output current, input voltage, input current and converter input current waveforms of the PWM AC Chopper shown in Figure 4.26. The chopper shows the same performance with the initial circuit given in Figure 4.21.

In appendixes the design of a non-isolated AC/DC, 1.5W power supply and an isolated 3 output 2W AC/DC power supply are given. These power supplies are implemented into the circuits to given in Figures 4.21 and 4.26 in order to allow the choppers to work independently.

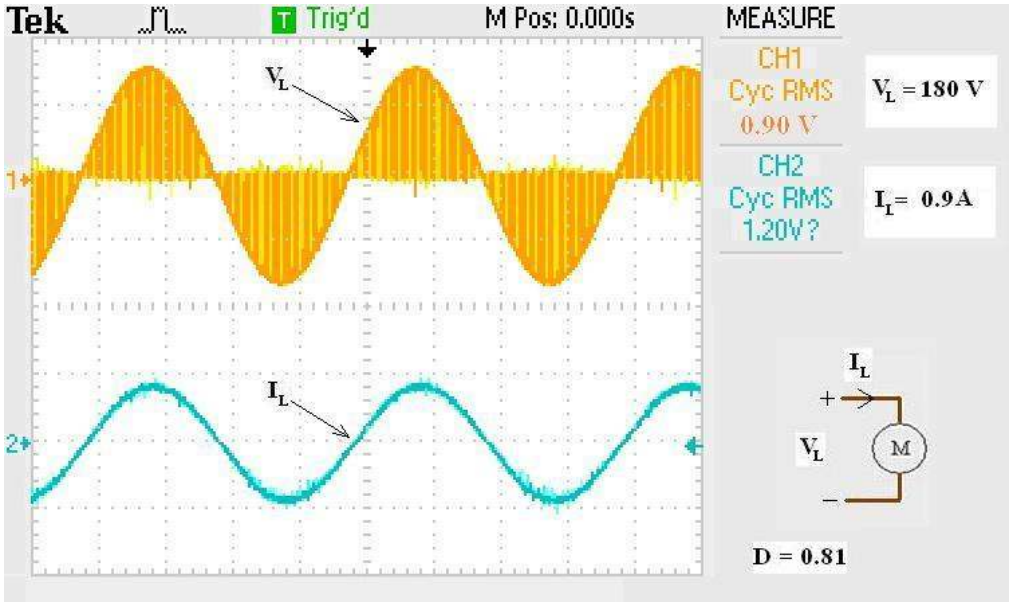


**Figure 4.27:** Output Voltage and Output Current (D = 0.81, Time Division = 5ms, Voltage Division = 200V, Current Division = 0.75A)

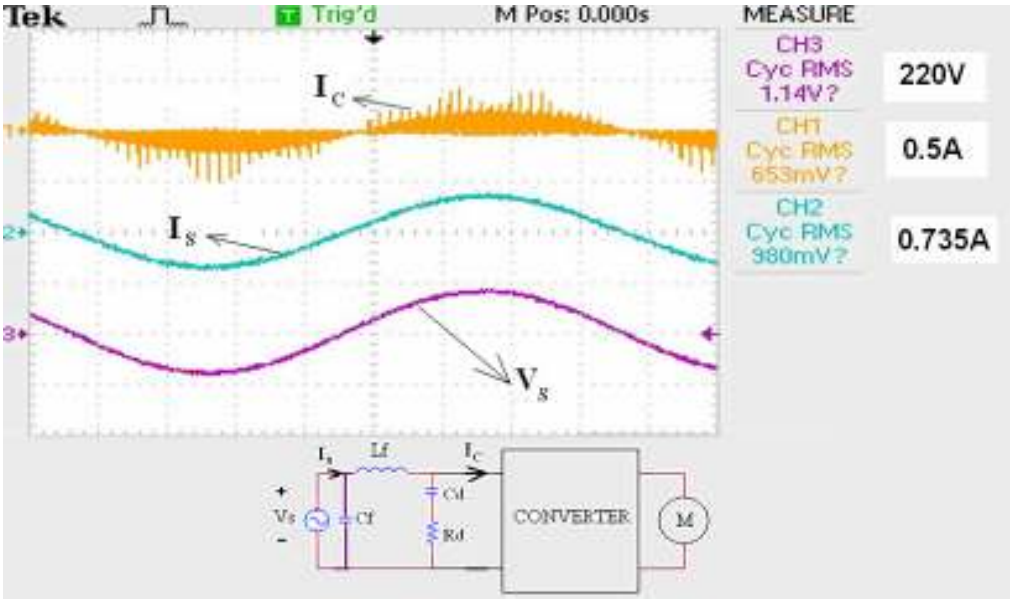


**Figure 4.28:** Input Voltage, Input Current and Converter Input Current (D = 0.51, Time Division = 2.5ms, Voltage Division = 400V, Current Division for $I_s$ (blue) = 1.5 A , Current Division for $I_c$ (yellow) = 3.75 )

## 5. TEMPERATURE CONTROL

The main purpose of this application was to produce a closed loop system which controls the speed of the single phase induction motor according to the temperature feedback from the control space.

A system which senses the temperature and assigns the appropriate voltage to PWM generator is needed. Temperature sensor is needed to measure the temperature. Many sensors can be found. Some of these sensors measure the temperature by changing its resistance for different temperature values. These sensors are called thermistor. There are two types of thermistors; NTC (Negative Temperature Constant) thermistor and PTC (Positive Temperature Constant) thermistor. The resistance of an NTC decreases for increasing temperature, for PTC the resistance decreases for decreasing temperatures. A Thermo-couple can be used as a sensor, where two different types of metals are connected at one end and the other ends are left open. The change of temperature causes a voltage difference at the open ends. Also integrated circuits to measure temperature can found. LM34 and LM35 are one of the most known temperature IC's. All sensors need a converter to convert the temperature signals they generate. Many different converters for these signals can be derived using operational amplifier. Two different circuits are introduced below to give an idea on these converters.

A circuit using an LM35 semiconductor temperature sensor and a flash converter to give necessary input signals to PWM generator in order to control the speed of the motor in steps. Figure 5.1 shows a general configuration of such a feedback unit.

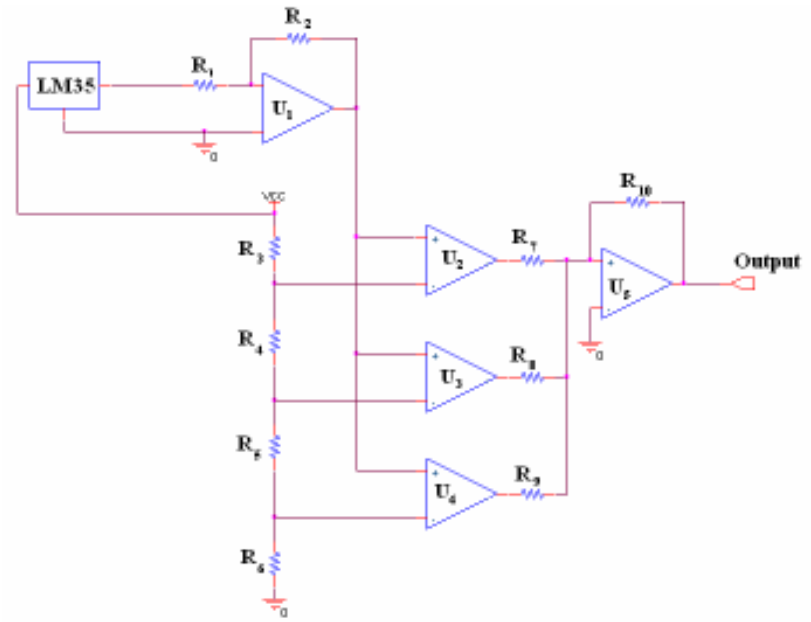


**Figure 5.1:** Flash Converter Feedback Circuit

This circuit has an advantage of controlling the motor speed in 3 steps. It can be stopped, turned in full speed or turned in half speed. The number of the comparators can be increased to control the speed in multiple steps if needed. Using multiple steps gives you the ability to control the motor in constant speeds for specified temperature intervals.

Another method can be done using a Negative Temperature Coefficient (NTC) thermistor for feedback. This method brings to advantages for use. One of them is smooth operating compared to the first method. The advantage is that it gives us to use the full speed range of the motor. The NTC is a resistor which changes the resistance value when temperature changes. A resistance-to-voltage converter with an output voltage range suitable for the PWM generator input can be used as feedback circuit. This can be done easily by an opamp converter shown Figure 5.2.

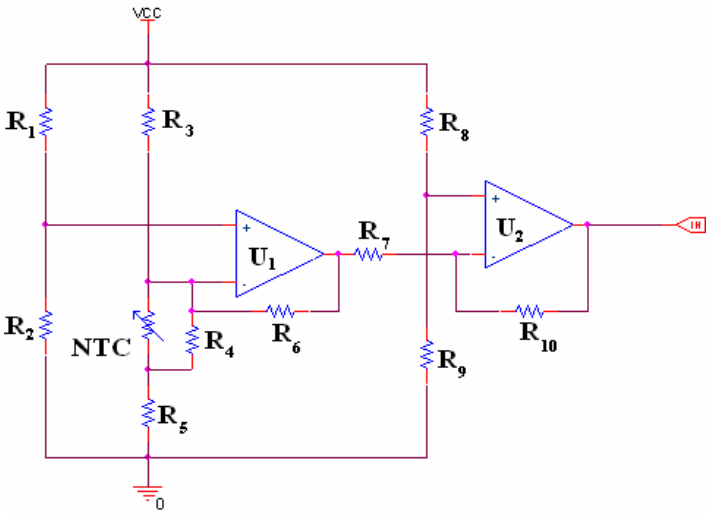


**Figure 5.2:** NTC Voltage Converter Circuit [4]

### 5.1 Design of Feed-back Circuit for Closed Loop Applications

For closed-loop operation a resistance-to-voltage converter shown in Figure 5.3 is designed for the PWM AC Chopper. The first step in designing such a feed-back network is to select a proper NTC for the application. For this project an NTC giving a 25 kΩ for 25ºC temperature was selected. The figure below shows the realized resistance-to-voltage converter. It has a simple structure using only one operational amplifier and it is suitable to produce the proper output 0.7 V – 3.3 V for the PWM generator UC3525.

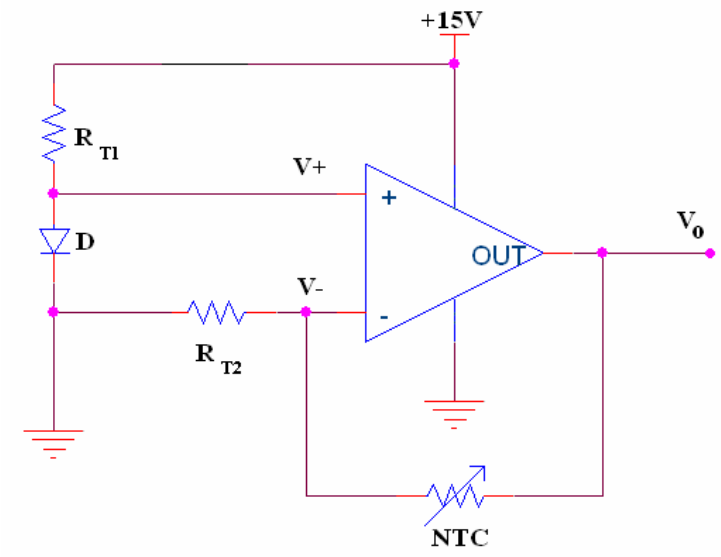


**Figure 5.3:** Resistance-to-Voltage Converter

The gain of the amplifier shown in Figure 5.3 is:

$$V_o = V_+(1+\frac{NTC}{R_{T2}}) \quad \textbf{(5.1)}$$

where $V_o$ is the output voltage, $NTC$ is the thermistor, $V_+$ is the operational amplifier non-inverting input voltage and $R_{T2}$ is resistor with fixed value.

As mentioned before UC3525 PWM generator reference voltage changes between 0.8V-3.3V. $V_+$ is fixed to 0.7V by a diode so that the bottom level of output would suit the requirements of UC3525. The resistor $R_{T1}$ is fixed 75kΩ to limit the current passing through the diode which also limits the current drawn from the DC source. NTC was selected to be 25kΩ at room temperature and $R_{T2}$ was calculated from Equation 5.1 to be 13kΩ. $R_{T2}$ limits the upper level of the output voltage to 3.3V. Figure 5.4 shows the output voltage characteristic for different NTC values.

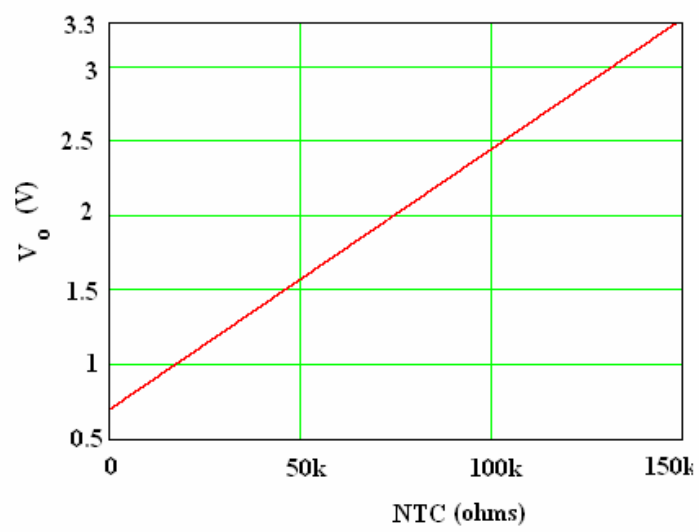


**Figure 5.4:** Change of Output Voltage for Different Resistance Values

The design was made assuming that the thermistor had a linear change of resistance for temperature changes. In practical the thermistor resistance changes exponentially with temperature. Like this, many applications based on resistance temperature characteristic require the use of a linearization network. This linearization can simply be achieved by implementing a resistor in parallel with the NTC. Figure5.5 shows the linearization of an NTC thermistor.

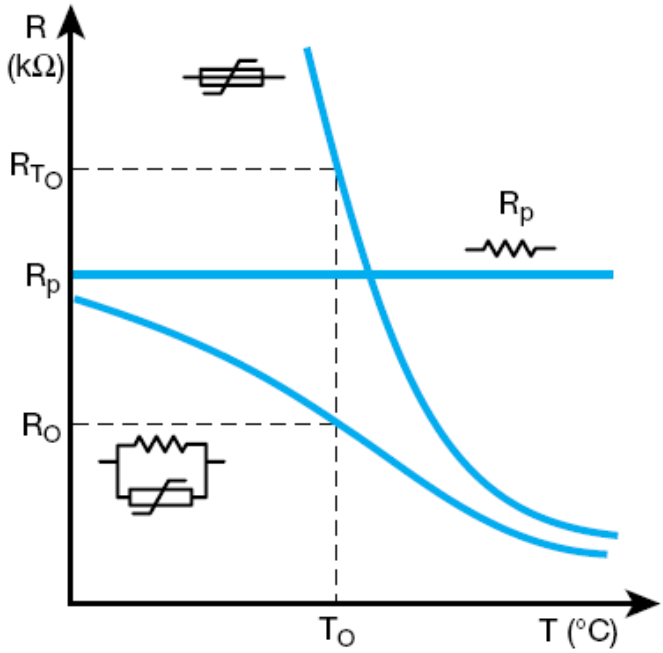


**Figure 5.5:** Linearization of Thermistor (AVX NTC Thermistor Catalog)

The calculation $R_p$ can be simply made as follows:

$$R_p = R_{To} \cdot \frac{B - T_0}{B + 2T_0} \tag{5.2}$$

where $R_p$ is the parallel linearization resistor, $R_{To}$ is the resistance of the NTC at 25ºC, $T_o$ is (25+273)ºK and $B$ is the sensitivity constant of the NTC specified by the manufacturer.

## 6. CONCLUSION

A high frequency PWM AC Chopper induction motor drive was designed and realized in this study for both domestic and industrial fan applications. This circuit can be used to control the motor speed according to the temperature reference.

In the first section of this thesis control techniques have been discussed. Then, the PWM AC Chopper was chosen for speed control. In the discussion part, The advantages of the PWM AC Chopper were given. These advantages were;

- Due to high frequency switching the PWM AC Chopper does not generate low frequency harmonics which are multiples of the 50Hz fundamental component.
- The harmonic distortions appear at higher frequencies that are actually multiples of the switching frequency. (In this thesis the switching frequency was selected 25kHz and the harmonics appear at 50kHz, 100kHz, 150kHz...)
- The PWM AC Chopper supplies the motor with continuous current.
- Simple to control compared with constant *V/f* control.
- Requires lesser amount of switching element compared with constant *V/f* control.
- The PWM AC Chopper is cost effective compared with the constant *V/f* control.

The PWM AC Chopper was designed by the help of Orcad Pspice design software in the third section. In this section a complete model for the PWM AC Chopper was derived and a single–phase induction motor model given in [7] is introduced. These simulations were made in order to see the performance of the PWM AC Chopper loaded by a dynamic motor model. The results lead to realization of the PWM AC Chopper.

n the fourth section harmonic analysis were made in order to reduce input voltage and input current harmonic distortions. Based on the standards [9] the design of a damped input filter has been made. Experimental results of the damped input filter have shown that the input voltage and input current harmonic distortions have been eliminated. The power consumption of the overall converter with damped input filter was also analyzed in this section. The results gave us that a small amount of power was lost in the input filter due to the damping resistor (the loss is about 12W for worst case). The measurement results also show that the power loss increases with decreasing duty cycle, also decreasing the efficiency. The efficiency for the PWM AC Chopper is good for duty cycles over 0.5 and can be tolerable for lower values. The efficiency must be considered when designing the temperature feed-back for closed loop operations.

The converter is supposed to work automatically to control the temperature. Section six gives the design of a feed-back for closed loop operation. The temperature feed-back is supplied by a NTC temperature sensor. In the realized circuit a resistance-to-voltage converter was used for feed-back.

The design of a filter inductor is introduced in Appendix A. The PWM AC Chopper is designed to work independently with out the use of external DC sources. Appendix B shows the design of low-cost low-power isolated and an isolated AC/DC power supplies for auxiliary circuits. Also a complete list of components used in the design of the PWM AC Chopper and simulation files are given in Appendix C.

For future works the PWM AC Chopper can be realized using microcontrollers or DSP units which can give a better design possibility of the control network. The design of a microprocessor based control network can give the possibility of applying sinusoidal PWM control which reduces the harmonic effects. A secondary work can be done on the input filter. The input filter affects the overall circuit in two important ways; it causes delay to the response of the control network and has power loss due to the damping resistance. The delay in response time is not important for this application but filter can be designed again in order to reduce the power loss. The chopper seems a very good solution for this application. Having better control and higher performance a constant volts-per-hertz control (V/f) for the motor drive should be designed. Also the use of vector control technique for single-phase induction motors can be thought as a future work.

## REFERENCES


[1] **Texas Instruments**, "Digital Signal Processing for AC Induction Motor". *Application Note* BPRA043.

[2] **Bose**, **B.K.** 1986. "Power Electronics and AC Drives", Prentice-Hall, New Jersey.

[3] **Jang, H. and Yoon D.**, 2003 "Space-Vector PWM Technique for Two-Phase Inverter-Fed Two-Phase Induction Motors", *IEEE* Transactıons on Industry Applications, **39**, no. 2, March/April 2003

[4] **Yucel E.**, 2006. "Bir Fazlı Sürekli Kondasatörlü Asenkron Motorlarda Hız Kontrolü", ("Speed Control of A Single-Phase Permanent-Split Capacitor Induction Motor"), *M.Sc. Thesis*, İ.T.Ü. Fen Bilimleri Enstitüsü, Istanbul

[5] **Erikson**, **R.W.** 2000. "Fundamentals of Power Electronics", Kluwer Academic Publishers.

[6] **Krause, P.C, Wasynczuk, O. and Sudoff**, **S.** 2002. "Analysis of Electric Machinery and Drive Systems", Wiley-Interscience, IEEE Press.

[7] **Faiz, J. and Keyhani**, **A.** 1997. "Pspice Simulation of Single Phase Induction Motors", Energy Conversion, *IEEE* Transactions on **14**, Issue 1, March 1999 Page(s): 86-92.

[8] **Tektronix**, "TDS1000B and TDS2000B Series Digital Storage Oscilloscope User Manuel".

[9] **TS EN 61000-3-2**, 2003 **"**Limits for harmonic current emissions (equipment input current up to and including 16A per phase)**",** *Standard*.

[10] **ST**, 2006. "Improved ST7LITE05 AC Chopper Driver Solution", AN2316 *Application Note*, ST Microelectronics.

[11] **Eri,kson**, **R. W.** 1999, “Optimal Single Resistor Daming of Input Filter”, Applied Power Electronics Conference and Exposition, 1999. APEC '99 Fourteenth Annual Volume 2, 14-18 March 1999 Page(s):1073 – 1079, **2**

[12] **Kassakian, J. G., Schlecht, M. F. and Verghese**, **G. C.,** 1991. “Principles of Power Electronics”, Addison-Wesley.

[13] **Rashid**, **M. H.** 1993. “Power Electronics, Circuits, Devices and Applications”, Prentice Hall.

[14] **Hoft**, **R. G.** 1986. “Semiconductor Power Electronics”, Van Nostrand Reinhold.

[15] **Mohan, N., Undeland, T. M. and Robbins**, **W.P.** 1995. “Power Electronics”, John Wiley and Sons.

[16] **Millman, J. and Grabel**, **A.** 1987. “Microelectronics” McGraw-Hill.

[17] **Yaakov, S.B. and Hadad**, **Y.** 2006, “A Four Quadrants HF AC Chopper with no Deadtime”, Applied Power Electronics Conference and Exposition, 2006. APEC '06. Twenty-First Annual *IEEE* 19-23 March 2006 Page(s):5 pp.

[18] **Chomat, M. and T. A. Lipo**, 2001. “Adjustable Speed Single Phase Induction Machine Drive with Reduced Number of Switches”, Industry Applications, *IEEE* Transactions on **39**, Issue 3, May-June 2003 Page(s):819 - 825

[19] **Bodur, H., Bakan, A. F. and Sarul**, **M. H.** 2000. “Universal Motor Speed Control with Current Controlled PWM AC Chopper by using a Microcontroller”, Industrial Technology 2000. Proceedings of *IEEE* International Conference on **1**, 19-22 Jan. 2000 Page(s):394 – 398, **2**

**APPENDIX A:** FILTER INDUCTOR DESIGN

In chapter 4, the value of the inductor used in the input filter was calculated and found to be 300 μH. In practical a 500 μH inductance was used in the PWM AC Chopper. The current passing through the inductor has an effective value of 0.9 A. In the design of an inductor the peak current passing through the inductor is important. The peak current $I_p$ is: $0.9 \times \sqrt{2}$ =1.3 A.

To avoid magnetic material from saturation the inductor was designed with an air-gap. The following equations show the determination of the air-gap volume from energy equations.

$$W = \frac{1}{2} \cdot L \cdot I_p^2 = \frac{1}{2} \times 500 \cdot 10^{-6} \times \left(0.9 \times \sqrt{2}\right)^2 = 0.000405\, Joules \quad \textbf{(A.1)}$$

$$W = \frac{1}{2} \cdot B \cdot H = \frac{1}{2} \cdot \frac{B_{maz}^2}{\mu_0} \cdot V_g \quad \textbf{(A.2)}$$

where $W$ is the energy stored in the inductor, $L$ is the inductor inductance, $I_p$ is the peak inductor current, $B_{max}$ is 0.8 Tesla for ferrite materials, $\mu_0$ is $4\pi \cdot 10^{-7}\, H/m$ and $V_g$ is the air-gap volume.

$$\frac{1}{2} \cdot \frac{0.8^2}{4\pi \cdot 10^{-7}} \cdot V_g = 0.000405\, Joules \quad \textbf{(A.3)}$$

$$V_g = 1.59043 \times 10^{-3}\, cm^3 \quad \textbf{(A.4)}$$

Since we know the necessary air-gap volume required, the air-gap length $l_g$ and the core dimensions can be determined by the help of Table A.1. If the air-gap length $l_g$ is selected to be 0.015 cm the cross-sectional area of the core is:

$$A_c = \frac{V_g}{l_g} = 0.106\, cm^2 \quad \textbf{(A.5)}$$

For $A_c$ 0.0106 $cm^2$ the EE12 core can be selected. The number of turns can be calculated as follows.

$$N = \sqrt{\frac{l_g \cdot L}{\mu_0 \cdot A_c}} = \sqrt{\frac{0.015 \times 10^{-2} \times 500 \times 10^{-6}}{4\pi \times 10^{-7} \times 0.106 \times 10^{-4}}} = 75 \; turns \qquad \textbf{(A.6)}$$

The winding area for EE12 is 0.085 $cm^2$. Assuming the current density of 5 $A/mm^2$ for the wire, the cross-sectional area for the wire to be used in inductor can be calculated,

$$A_{wire} = \frac{1.3\,(A)}{5(A/mm^2)} = 0.26 \; mm^2 \qquad \textbf{(A.7)}$$

The diameter of the wire for this cross-sectional area is found to be 0.57 *mm*. From the wire cross-sectional area and the number of turn the winding area can be calculated in order check if the turns fit EE12 core. Assuming the winding factor $k_w$ to be 1.2 the total area of the winding is:

$$Winding\ Area = k_w \cdot N \cdot A_{wire} = 1.2 \times 75 \times 0.26 \times 10^{-2} = 0.230 cm^2 \qquad \textbf{(A.8)}$$

As it can be seen the windings cannot fit the EE12 core so EE16 is selected and the number of turns is recalculated. The core cross-sectional area ($A_c$) for EE16 is 0.19

$$N = \sqrt{\frac{0.015 \times 10^{-2} \times 500 \times 10^{-6}}{4\pi \cdot 10^{-7} \times 0.19 \times 10^{-4}}} = 56 \; turns \qquad \textbf{(A.9)}$$

$$Winding\ Area = 1.2 \times 56 \times 0.26 \times 10^{-2} = 0.174 mm^2 \qquad \textbf{(A.10)}$$

Now, the windings fit the EE16 core. Then, the filter inductor is designed with a EE16 core with 56 turns of 0.26 *mm* diameter wires. The serial resistance of this inductor is,

$$R_S = \frac{\rho \cdot MLT \cdot N}{A_{wire}} = \frac{1.724 \times 10^{-6} \times 54 \times 3{,}4}{0.26 \times 10^{-2}} = 0.13\Omega \qquad \textbf{(A.11)}$$

where $\rho$ is the specific conductivity of the copper, *MLT* is the mean length per turns of winding, $N$ is the number of turns, $A_{wire}$ is the wire cross-sectional area.

**Table A.1:** EE Core Data

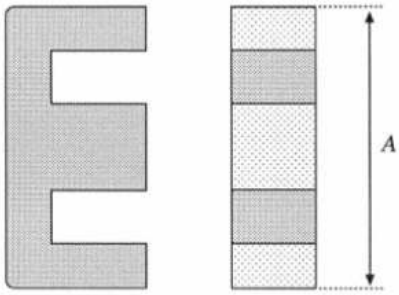


| Core type (A) (mm) | Geometrical constant $K_g$ ($cm^5$) | Geometrical constant $K_{gfe}$ ($cm^x$) | Cross-sectional area $A_c$ ($cm^2$) | Bobbin winding area $W_A$ ($cm^2$) | Mean length per turn $MLT$ (cm) | Magnetic path length $\ell_m$ (cm) | Core weight (g) |
|---|---|---|---|---|---|---|---|
| EE12 | $0.731 \cdot 10^{-3}$ | $0.458 \cdot 10^{-3}$ | 0.14 | 0.085 | 2.28 | 2.7 | 2.34 |
| EE16 | $2.02 \cdot 10^{-3}$ | $0.842 \cdot 10^{-3}$ | 0.19 | 0.190 | 3.40 | 3.45 | 3.29 |
| EE19 | $4.07 \cdot 10^{-3}$ | $1.3 \cdot 10^{-3}$ | 0.23 | 0.284 | 3.69 | 3.94 | 4.83 |
| EE22 | $8.26 \cdot 10^{-3}$ | $1.8 \cdot 10^{-3}$ | 0.41 | 0.196 | 3.99 | 3.96 | 8.81 |
| EE30 | $85.7 \cdot 10^{-3}$ | $6.7 \cdot 10^{-3}$ | 1.09 | 0.476 | 6.60 | 5.77 | 32.4 |
| EE40 | 0.209 | $11.8 \cdot 10^{-3}$ | 1.27 | 1.10 | 8.50 | 7.70 | 50.3 |
| EE50 | 0.909 | $28.4 \cdot 10^{-3}$ | 2.26 | 1.78 | 10.0 | 9.58 | 116 |
| EE60 | 1.38 | $36.4 \cdot 10^{-3}$ | 2.47 | 2.89 | 12.8 | 11.0 | 135 |
| EE70/68/19 | 5.06 | $75.9 \cdot 10^{-3}$ | 3.24 | 6.75 | 14.0 | 18.0 | 280 |

**APPENDIX B:** DESIGN OF AUXILIARY POWER SUPPLIES

The PWM AC Chopper is designed to work independently from external DC sources. Appendix B gives the design of isolated and an-isolated low-cost low-power AC/DC power supplies for auxiliary circuits. Both designs were made using ST microelectronics VIPer Design Software for isolated and an-isolated power supplies.

## B.1 An-Isolated AC/DC Power Supply

ST microelectronics presents a power switch for auxiliary power supplies. By the use of VIPer series power switches the user is capable of designing the desired power supplies. The power supply designed to feed the auxiliary circuits in Figure 4.24 is shown in Figure B.1 and the list of components are given in Table B.1.

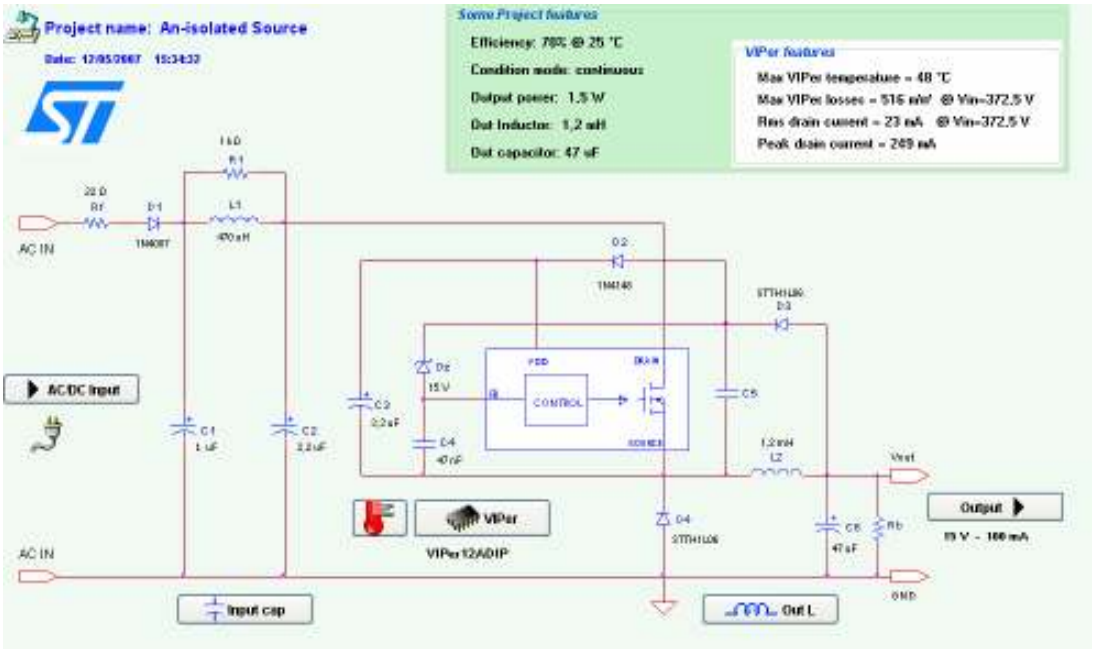


**Figure B.1:** An-Isolated Buck Converter

## B.2 Isolated AC/DC Power Supply

By using the same power switch mentioned in B.1 a flyback topology isolated DC power supply has been designed. Figure B2 shows the designed isolated AC/DC power supply used to feed auxiliary circuits shown in Figure 4.19.

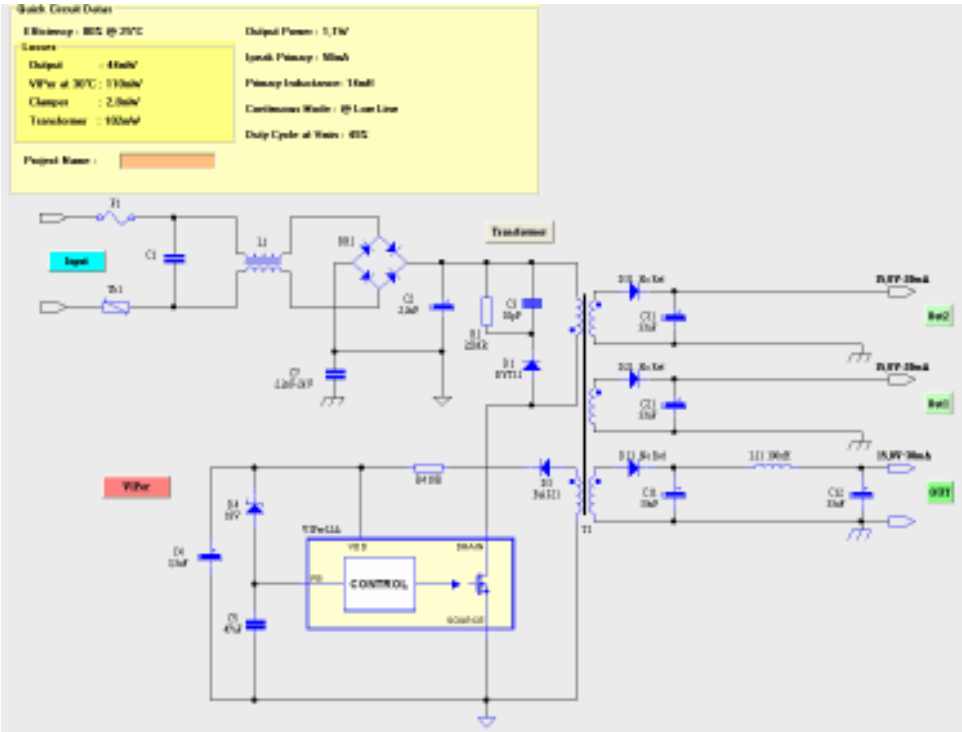


**Figure B.2:** Isolated Fly Back Converter using VIPer20A

**APPENDIX C:** LIST OF COMPONENTS AND PSPICE .cir FILES

**Table C.1:** Component Ratings of Realized PWM AC Chopper (Figure 4.21)

| COMPONENTS | NAMES | RATINGS |
|---|---|---|
| M1, M2 M3, M4 | IXYS IXFH26N50 Power MosFETs | 500V 26A |
| Lf | Filter Inductor | 500 uH, 3A |
| Cf | Filter Capacitor | 1 uF, 630 V |
| Cd | Damping Capacitor | 0.1 uF, 630 V |
| Rd | Damping Resistor | 235 Ω, 10 W |
| R1+Rvar | Multi-turn Variable Resistor | 20 kΩ, ½ W |
| R2 | Resistor | 2.2 kΩ, 1/2 W |
| R3 | Resistor | 5.1 kΩ, 1/2 W |
| R4, R5, R6, R7 | Resistor | 1 kΩ, ½ W |
| R8,R9 | Resistor (between MosFET Gate - TLP251) | 10 Ω |
| C1 | Capacitor | 10 nF, 16V |
| C2 | Capacitor | 1 nF, 16V |
| C3, C4 | Capacitor | 100 nF, 16 V |
| UC 3525 | PWM Generator | |
| TC 428 | MosFET Driver | |
| TLP 251 | Opto-coupler | |

**Table C.2:** Component Ratings of Realized PWM AC Chopper (Figure 4.26)

| COMPONENTS | NAMES | RATINGS |
|---|---|---|
| M1, M2 M3, M4 | IRF840 Power MosFET | 500V 8A |
| Lf | Filter Inductor | 500 uH, 3A |
| Cf | Filter Capacitor | 1 uF, 630 V |
| Cd | Damping Capacitor | 0.1 uF, 630 V |
| Rd | Damping Resistor | 235 Ω, 10 W |
| R1+Rvar | Multi-turn Variable Resistor | 20 kΩ, ½ W |
| R2 | Resistor | 2.2 kΩ, ½ W |
| R3 | Resistor | 5.1 kΩ, ½ W |
| R4, R5 | Resistor | 1 kΩ, 1/2 W |
| R6 | Resistor | 10 Ω, 1/2 W |
| C1 | Capacitor | 10 nF, 16V |
| C2 | Capacitor | 1 nF, 16V |
| C3, C4 | Capacitor | 100 nF, 16 V |
| C5 | Capacitor | 1 uF, 30 V |
| C6,C7 | Capacitor, output of pulse transformer for clamper | 1 uF, 30V |
| Z1,Z2 | Zener Diode, output of pulse transformer for clamper | 15V |
| R7,R8 | Resistance, output of pulse transformer for clamper | 2 kΩ, 1/2 W |
| UC 3525 | PWM Generator | |
| TC 428 | MosFET Driver | |
| SD250-3 | Pulse Transformer | |

**Appendix C.1:** Program File: Pspice Circuit File used in Simulation

```
*PWM AC Chopper Single Phase Induction Motor Drive

*AC Chopper
    VAC 20 0 sin(0 155 60 0 0 0)
    XS1 20 21 16 13 mos_switch
    XS2 21 0  17 15 mos_switch

*Permanent Capacitor Single Phase Induction Motor
    XIM 20 Z PCIM
    Rb Z 30 0.000024
    Lj 30 0 0.0074

*MosFET Driver
    E1 12 13 3 11 1
    E2 14 15 11 0 1
    RE1 12 16 47
    RE2 14 17 47
```

```
*PWM Generator
    VCC 3 0 DC 15V
    VEE 0 4 DC 15V
    Vref 8 0 0
    R1 5 1 10k
    R2 1 6 9k
    R3 5 7 1k
    R4 5 0 1k
    R5 7 6 100k
    R6 9 10 10k
    R7 3 11 1k
    C1 7 6 0.01u IC=0
    X1 1 0 3 4 5 lm675
    X2 0 7 3 4 6 lm675
    X3 6 8 3 4 9 lm675
    Q1 11 10 0 npntr
.model npntr npn()

*---------- OPAMP Pspice Models ------------------
* Connections: non-inverting input
*              | inverting input
*              | | positive power supply
*              | | | negative power supply
*              | | | | output
*              | | | | |
.subckt lm675 1 2 3 4 5
    c1 11 12 8.660E-12
    c2 6 7 15.00E-12
    dc 5 53 dx
    de 54 5 dx
    dlp 90 91 dx
    dln 92 90 dx
    dp 4 3 dx
    egnd 99 0 poly(2),(3,0),(4,0) 0 .5 .5
    fb 7 99 poly(5) vb vc ve vlp vln 0 7.717E9 -7E9 7E9 7E9 -7E9
    ga 6 0 11 12 518.4E-6
    gcm 0 6 10 99 16.40E-9
    iee 3 10 dc 120.4E-6
    hlim 90 0 vlim 1K
    q1 11 2 13 qx
    q2 12 1 14 qx
    r2 6 9 100.0E3
    rc1 4 11 1.929E3
    rc2 4 12 1.929E3
    re1 13 10 1.493E3
    re2 14 10 1.493E3
    ree 10 99 1.661E6
    ro1 8 5 50.00E-3
    ro2 7 99 50.00E-3
    rp 3 4 2.796E3
```

```
    vb 9 0 dc 0
    vc 3 53 dc 4
    ve 54 4 dc 4
    vlim 7 8 dc 0
    vlp 91 0 dc 3.000E3
    vln 0 92 dc 3.000E3
.model dx D(Is=800.0E-18)
.model qx PNP(Is=800.0E-18 Bf=300)
.ends

*----------------- Bi-Directional Switch Model ------------------------
.SUBCKT mos_switch 11 12 13 14
    D1 14 11 diyot
    D2 14 12 diyot
    D3 11 15 diyot
    D4 12 15 diyot
    M1 15 13 14 14 IRF240
.model diyot D(Is=14.11n N=1.984 Rs=33.89m
+ Ikf=94.81 Xti=3 Eg=1.11
+ Cjo=25.89p Vj=0.3245
+ Fc=0.5 Bv=1500 Ibv=10u
+ Tt=5.7u)
.model IRF240 NMOS(Level=3 Gamma=0 Delta=0 Eta=0 Theta=0 Kappa=0.2
Vmax=0 Xj=0
+Tox=100n Uo=600 Phi=.6 Rs=5.466m Kp=20.82u W=.44 L=2u Vto=3.814
+Rd=97.84m Rds=888.9K Cbd=1.813n Pb=.8 Mj=.5 Fc=.5 Cgso=1.977n
+Cgdo=490.5p Rg=3.604 Is=5.191p N=1 Tt=312n)
.ends

*--------- Single Phase Induction Motor Model ---------------------------
.subckt PCIM 1 17
    Rq 4 5 4.12
    Llq A 4 5.6m IC=0
    LMm 3 0 177m IC=0
    Llm 2 B 7.4m IC=0
    Rm 1 2 2.02
    Rcs C 7 1
    Cs 7 8 50u IC=0
    Ra 8 9 7.14
    Lla 9 10 8.5m IC=0
    LMa 10 0 246m IC=0
    Lld D 11  7.8m IC=0
    Rd 11 12 5.74
    Vx A 3 0
    Vy B 3 0
    Vz 1 C 0
    Vt D 10 0
    H11 5 6 poly(2) vtl vz 0 0 0 0 0.416
    H12 6 0 poly(2) vtl vt 0 0 0 0 0.430
    H13 13 12 poly(2) vtl vy 0 0 0 0 0.416
```

```
    H14 0 13  poly(2) vtl vx 0 0 0 0 0.430
    Vtl 16 17 0
    H1 16 14 poly(2) Vy Vt 0 0 0 0 0.5
    H2 0 14 poly(2) Vx Vz  0 0 0 0 0.5
.ends
*--------------------------------------------------------------------------------
.TRAN 1u 1
.PROBE
.END
```

**APPENDIX D:** PICTURES OF REALIZED PWM AC CHOPPER AND THE INDUCTION MOTOR USED IN EXPERINMENTS

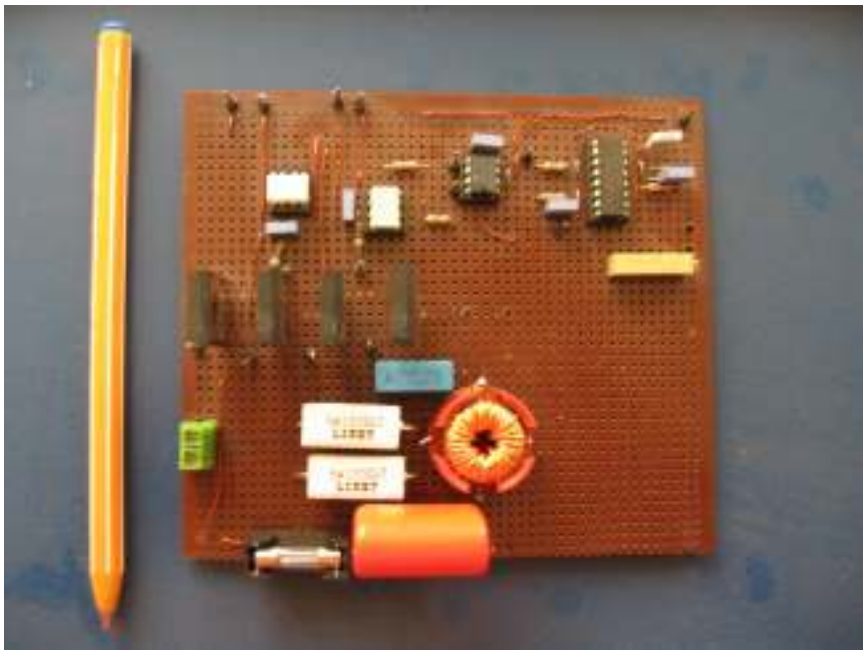

**Figure D.1:** PWM AC Chopper Realized with Opto-couplers

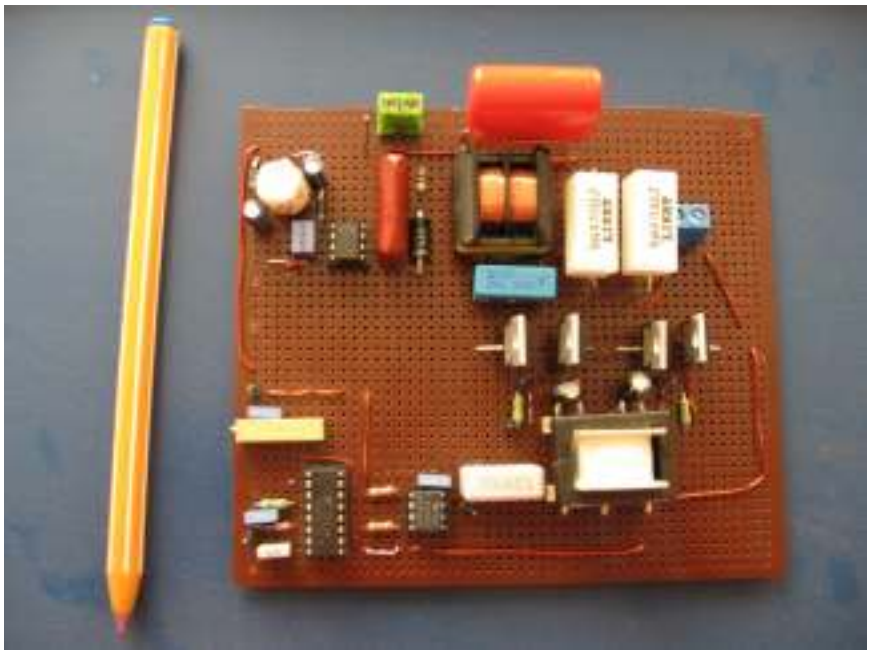

**Figure D.2:** PWM AC Chopper Realized with Pulse Transformer

**Figure D.3:** Single Phase Induction Motor Used in Experiments (BAHÇİVAN ELECTRIC MOTORS)


**Figure D.4:** Ratings of the Single-Phase Induction Motor Pictured in Figure D.3 (BAHÇİVAN ELECTRIC MOTORS)

## BIOGRAPHY

Mustafa Murat Bilgiç was born in Istanbul on July 18th, 1981. He completed high school education in Adnan Menderes Anatolian Lycée on June 1997. In 1999 he entered Yeditepe University and graduated on January 2004 from Electric–Electronics Engineering. He began his MSc. Studies in Istanbul Technical University in 2004. He is still an attending student in Istanbul Technical University. His areas of interests are power electronics and motor drives.